

# TPGDiff: Hierarchical Triple-Prior Guided Diffusion for Image Restoration

Yanjie Tu<sup>1</sup>, Qingsen Yan<sup>1,2†</sup>, Axi Niu<sup>1</sup>, Jiacong Tang<sup>1</sup>

<sup>1</sup> Northwestern Polytechnical University

<sup>2</sup> Shenzhen Research Institute of Northwestern Polytechnical University

{yanjetu, tangjiacong}@mail.nwpu.edu.cn; {qingsenyan, nax}@nwpu.edu.cn

## Abstract

All-in-one image restoration aims to address diverse degradation types using a single unified model. Existing methods typically rely on degradation priors to guide restoration, yet often struggle to reconstruct content in severely degraded regions. Although recent works leverage semantic information to facilitate content generation, integrating it into the shallow layers of diffusion models often disrupts spatial structures (*e.g.*, blurring artifacts). To address this issue, we propose a Triple-Prior Guided Diffusion (TPGDiff) network for unified image restoration. TPGDiff incorporates degradation priors throughout the diffusion trajectory, while introducing structural priors into shallow layers and semantic priors into deep layers, enabling hierarchical and complementary prior guidance for image reconstruction. Specifically, we leverage multi-source structural cues as structural priors to capture fine-grained details and guide shallow layers representations. To complement this design, we further develop a distillation-driven semantic extractor that yields robust semantic priors, ensuring reliable high-level guidance at deep layers even under severe degradations. Furthermore, a degradation extractor is employed to learn degradation-aware priors, enabling stage-adaptive control of the diffusion process across all timesteps. Extensive experiments on both single- and multi-degradation benchmarks demonstrate that TPGDiff achieves superior performance and generalization across diverse restoration scenarios. Our project page is: [TPGDiff](#).

## 1. Introduction

Image restoration is a fundamental task in low-level computer vision, aiming to reconstruct high-quality images from degraded low-quality observations. It has been widely applied to various scenarios, including image denoising [92, 115, 116], deblurring [71, 81, 83], desnowing [12, 13, 51], dehazing [23, 80, 90], deraining [11, 14, 42], and low-light

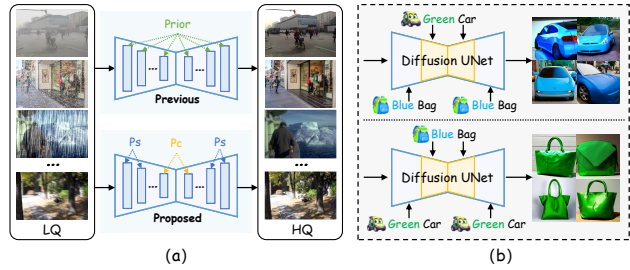


Figure 1. (a) Existing methods inject prior information uniformly into the diffusion model, whereas our approach adopts a hierarchical strategy, distributing distinct priors across specific layers of the network. (b) The generation results of diffusion models are largely governed by representations encoded in the deep layers of the network, which play a dominant role in determining the final reconstruction.

enhancement [78, 98, 100]. Traditional methods typically focus on addressing a single type of degradation [10, 25, 33, 41, 46, 123], necessitating the training of separate models for different restoration tasks. However, real-world images often suffer from multiple coupled degradations simultaneously, making task-specific restoration pipelines inefficient and limiting scalability and generalization. To address this issue, recent studies have shifted attention to all in one image restoration [2, 39, 53, 86, 88, 107, 119, 120], which aims to handle multiple degradation types using a single model, thereby improving practicality and general applicability.

Under the all in one image restoration framework, different degradation types often exhibit markedly distinct statistical properties and corruption patterns, making it challenging to effectively distinguish diverse degradation scenarios by relying solely on a single Restoration model. To alleviate this limitation, a substantial body of existing work [28, 38, 65, 85, 106, 114] introduces degradation-related information as conditional signals, learning representations associated with degradation types or degradation severity from low-quality images to guide and modulate the restoration behavior under different degradation conditions.

†Corresponding author.

However, degradation information primarily characterizes low-level corruption patterns, and its representation is typically weakly correlated with high-level semantic content. Under complex degradation conditions, relying solely on degradation cues often fails to ensure semantic plausibility of the restored results, leading to issues such as content shift or semantic distortion [66]. To address this, several recent works [2, 35, 54, 56, 69, 86, 94, 96, 102, 119, 121] leverage pretrained models to extract high-level semantic priors, which are integrated into the restoration network to enforce semantic consistency.

Despite ensuring content consistency, abstract semantic priors often lack the granularity to preserve local geometries. Consequently, their premature integration can compromise spatial integrity, leading to structural blurring or misalignments. Under complex degradation conditions or severe detail loss, relying solely on semantic information often fails to guarantee pixel-level spatial consistency, leading to structural artifacts such as edge discontinuities or geometric distortions. To bridge this gap, several studies incorporate structural priors, such as edge maps or segmentation masks, to assist diffusion models in specific tasks [59, 61, 117]. These efforts demonstrate that structural cues provide geometric constraints that are highly complementary to semantic priors. Meanwhile, as the number of incorporated priors increases, effectively exploiting heterogeneous priors remains a key challenge. Most existing methods employ a uniform prior-injection strategy, implicitly assuming that priors elicit similar responses across network layers. However, diffusion models exhibit layers-dependent modeling behaviors [44, 84]: shallow layers are primarily responsible for encoding local structures and low-level statistics, whereas deeper layers prioritize the synthesis of global semantics and high-level content, as illustrated in Figure 1.

Motivated by these observations, we leverage the layer-wise characteristics of the UNet backbone in diffusion models to enable feature-prior coordination. Specifically, semantic priors are applied to deep layers to constrain global content, while structural priors are injected into shallow layers to preserve local geometric details. Building on this design, we propose TPGDiff (Triple-Prior Guided Diffusion), a unified image restoration framework that integrates semantic, structural, and degradation priors. By adaptively deploying heterogeneous priors across both the network and the denoising process, TPGDiff achieves a favorable balance between perceptual realism and structural fidelity.

- We propose TPGDiff, a novel prior-guided all-in-one image restoration framework that integrates *semantic*, *structural*, and *degradation* priors to jointly enhance restoration fidelity, perceptual realism, and visual consistency.
- We design a *layer-aware prior coordination* strategy that assigns semantic priors to deep layers and structural pri-

ors to shallow layers, enabling effective prior utilization while mitigating semantic drift and preserving local geometric integrity.

- Extensive experiments on both single- and multi-degradation image restoration benchmarks demonstrate that TPGDiff consistently outperforms state-of-the-art methods.

## 2. Related Work

### 2.1. All in One Image Restoration

All in One image restoration aims to handle multiple image degradations with a single model, thereby avoiding the efficiency and generalization issues caused by training separate models for different tasks. However, due to the substantial differences in the causes and manifestations of various degradations, this problem is inherently more challenging than task-specific image restoration [6, 26, 36, 43]. To address this challenge, existing methods typically introduce degradation-related information as conditional signals to guide the model in adaptively adjusting its restoration behavior under different degradation scenarios. For instance, AirNet [38] employs contrastive learning to obtain discriminative degradation representations, PromptIR [65] encodes degradation information using learnable prompts, and NDR [119] achieves dynamic degradation modeling through degradation queries and attention mechanisms. Furthermore, several studies incorporate semantic or content priors to alleviate semantic distortion under severe degradation conditions. For example, Perceive-IR [119] constructs a generic restoration framework via quality-driven prompt learning and difficulty-adaptive perceptual loss, while MaskDCPT [29] enhances generalization through masked image modeling and weakly supervised degradation classification pretraining. Despite these advances, existing methods primarily rely on deterministic mappings, which struggle to model the high-frequency diversity and stochastic uncertainty inherent in complex restoration tasks, often leading to over-smoothed results.

### 2.2. Diffusion-based Image Restoration

In recent years, diffusion models (DMs) have achieved remarkable progress in image generation and editing due to their stable training dynamics and superior generation quality [27, 74, 77, 79], and have been gradually introduced into image restoration tasks [21, 87, 120]. To further improve restoration performance, existing methods typically incorporate conditional information to guide the reverse diffusion process, where the conditions may take the form of degradation-related features, semantic embeddings, or task-specific guidance signals. For example, MPerceiver [2] achieves unified diffusion-based image restoration for multiple degradation tasks through dual-branch conditional.

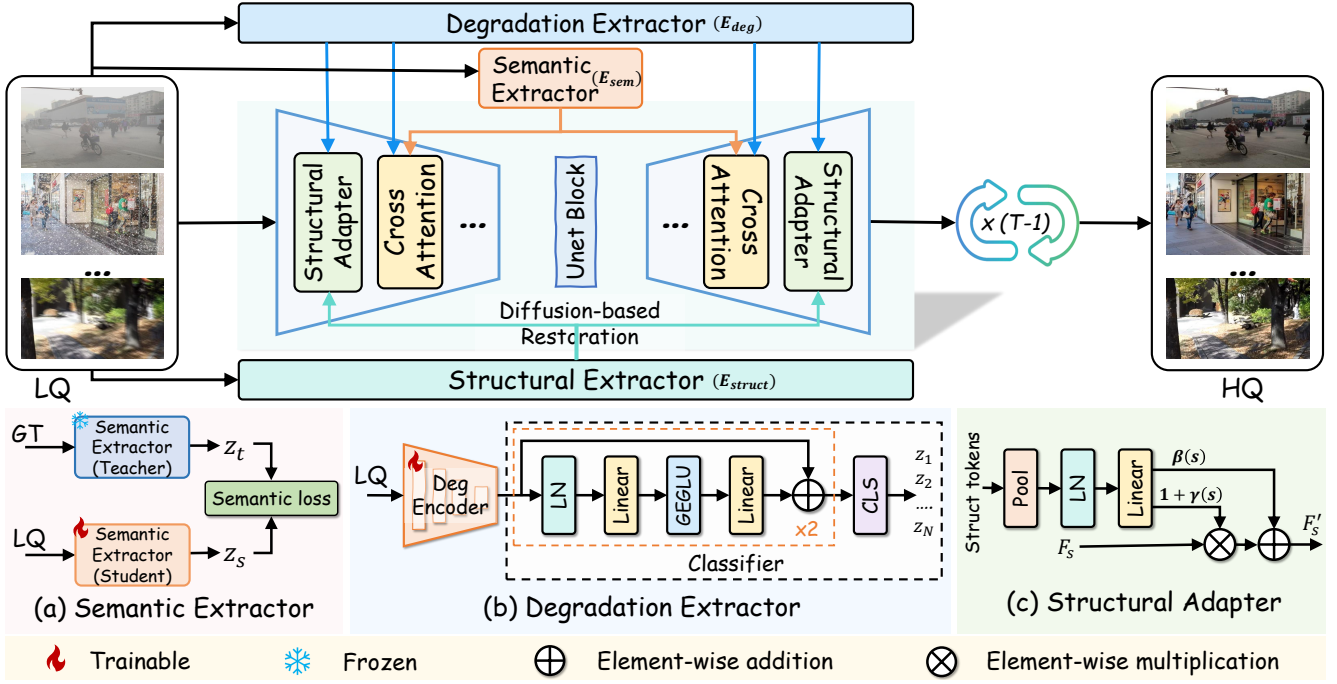


Figure 2. Overall architecture of TPGDiff. The framework explicitly models three types of priors from a low-quality input image and integrates them into a diffusion-based restoration network: (a) a *semantic extractor* that learns semantic representations via teacher-student distillation, (b) a *degradation extractor* that captures degradation-related characteristics, and (c) a *structural adapter* that injects structural priors into the diffusion model through an adapter module.

Diff-Plugin [50] supports multiple image restoration tasks by driving task selection with language instructions and activating different plug-in components. DA-CLIP [54] guides diffusion models to perform multi-task restoration using degradation-type descriptions and semantic prompts as conditions. DiffRes [86] extracts degradation-aware representations from pretrained vision-language models and modulates the diffusion process via feature differencing and adapter-based conditioning. While diffusion models offer stronger generative priors, current approaches typically adopt a unified injection strategy. This overlooks the functional divergence of hierarchical features, failing to resolve the conflicts between global semantics and local structural integrity.

### 3. Method

In this section, we present TPGDiff, a unified diffusion-based framework for all-in-one image restoration. TPGDiff employs a *triple-prior learning* mechanism to capture complementary semantic, structural, and degradation cues. Instead of uniform prior injection, these priors are *layer-aware coordinated* across the UNet backbone, aligning prior types with corresponding feature representations. This design enforces global content consistency while preserving local geometric details under diverse degradation con-

ditions.

#### 3.1. Overview of the Proposed Framework

As illustrated in Figure 2, given a low-quality input  $x_{LQ}$ , TPGDiff first extracts semantic, structural, and degradation priors using dedicated modules. These priors are layer-aware coordinated within the diffusion model to guide high-fidelity image restoration.

Specifically, a semantic encoder learns semantic representations from  $x_{LQ}$  via a teacher-student distillation scheme,

$$\mathbf{z}_{sem} = E_{sem}(x_{LQ}), \quad (1)$$

while structural and degradation extractors capture corresponding priors,

$$\mathbf{z}_{struct} = E_{struct}(x_{LQ}), \quad \mathbf{z}_{deg} = E_{deg}(x_{LQ}), \quad (2)$$

where details of each prior extractor are presented in subsequent subsections.

For image restoration, we adopt the IR-SDE diffusion [55] framework and recover the high-quality image by solving the reverse stochastic differential equation. Let  $\mathbf{x}(t)$  denote the diffusion trajectory at time  $t$ , the reverse process

is given by:

$$\begin{aligned} d\mathbf{x} = & \left[ \theta_t(\boldsymbol{\mu} - \mathbf{x}) - \sigma_t^2 s_{\theta}(\mathbf{x}, t; \boldsymbol{\mu}, \mathbf{z}_{\text{sem}}, \mathbf{z}_{\text{struct}}, \mathbf{z}_{\text{deg}}) \right] dt \\ & + \sigma_t d\hat{\mathbf{w}}. \end{aligned} \quad (3)$$

where  $\theta_t$  and  $\sigma_t$  are time-dependent coefficients and  $\hat{\mathbf{w}}$  denotes the reverse-time Wiener process. The score function  $s_{\theta}(\cdot)$  is conditioned on multiple priors, allowing the reverse diffusion process to jointly exploit semantic, structural, and degradation information during progressive denoising.

### 3.2. Semantic Prior Modeling

**Semantic Prior Learning.** Semantic priors are employed to constrain the high-level content consistency of restoration results and should be decoupled from specific degradation information wherever possible. However, when semantic representations are extracted directly from low-quality images, they are often compromised by degradation factors such as noise and blurring [121]. To obtain degradation-insensitive semantic representations, we employ a distillation-based semantic learning strategy, transferring stable semantic information from high-quality images through a teacher-student framework. As illustrated in Figure 2(a), we employ a dual-encoder [72] distillation framework: the teacher encoder  $E_T$  extracts reference semantic features from  $x_{\text{GT}}$ , while the student encoder  $E_{\text{sem}}$  aims to recover equivalent representations from the degraded input  $x_{\text{LQ}}$

$$\mathbf{z}_t = E_T(x_{\text{GT}}), \quad \mathbf{z}_s = E_{\text{sem}}(x_{\text{LQ}}), \quad (4)$$

where  $E_T(\cdot)$  is a pretrained encoder with frozen parameter, and  $E_{\text{sem}}(\cdot)$  is updated during training. We align their semantic spaces via a cosine similarity distillation loss:

$$\mathcal{L}_{\text{sem}} = \frac{1}{B} \sum_{i=1}^B \left( 1 - \frac{\mathbf{z}_s^{(i)} \cdot \mathbf{z}_t^{(i)}}{\|\mathbf{z}_s^{(i)}\|_2 \|\mathbf{z}_t^{(i)}\|_2} \right), \quad (5)$$

where  $\mathbf{z}_s^{(i)}$  and  $\mathbf{z}_t^{(i)}$  denote the semantic feature representations of the  $i$ -th sample produced by the student and teacher encoders, respectively. This constraint encourages the student encoder to distill high-level, degradation-invariant content representations, even under severe low-quality conditions. Once optimized, the features produced by  $E_{\text{sem}}$  serve as robust semantic priors, anchoring the subsequent restoration process with consistent content guidance.

**Semantic-guided Deep Attention.** Semantic priors are primarily used to constrain the global content consistency of the restored results, they are well suited for the deep modules of the diffusion network, which are intrinsically associated with high-level representations. Guided by this principle, we integrate the semantic prior  $\mathbf{z}_s$  as conditional context  $\bar{\mathbf{C}}$ , enabling it to interact with intermediate feature

maps via cross-attention mechanisms within the deep layers of the UNet. Specifically, the intermediate spatial features are denoted as  $\bar{\mathbf{X}} \in \mathbb{R}^{L \times D}$ , while the projected semantic prior forms a context sequence  $\bar{\mathbf{C}} \in \mathbb{R}^{M \times D}$ . The output of the cross-attention is defined as:

$$\mathbf{O} = \text{CA}(\bar{\mathbf{X}}, \bar{\mathbf{C}}) = \text{softmax} \left( \frac{\mathbf{Q}\mathbf{K}^{\top}}{\sqrt{d}} \right) \mathbf{V}. \quad (6)$$

where  $\mathbf{Q} = \bar{\mathbf{X}}W_q$ ,  $\mathbf{K} = \bar{\mathbf{C}}W_k$ , and  $\mathbf{V} = \bar{\mathbf{C}}W_v$ , with  $W_q$ ,  $W_k$ , and  $W_v$  denoting linear projection matrices. This design enables each spatial location to adaptively retrieve relevant cues from the global semantic context. Consequently, it effectively mitigates semantic drift during the diffusion sampling process, ensuring object integrity and overall content consistency.

### 3.3. Structural Prior Modeling

**Structural Prior Learning.** Under complex degradation conditions, the geometric structure and boundary morphology of images are often severely compromised, making it difficult to recover fine-grained structural information solely from semantic priors. To this end, we introduce structural priors to capture both local and global geometric cues, thereby facilitating accurate image restoration. As illustrated in Figure 3, we extract three categories of complementary structural cues from the degraded input: depth maps  $x^{\text{Dep}}$  to represent global geometric layouts, segmentation maps  $x^{\text{Seg}}$  to enforce regional consistency and object boundaries, and Difference-of-Gaussians (DoG) features  $x^{\text{DoG}}$  to capture fine-grained contours and high-frequency details. Depth and segmentation maps are extracted using off-the-shelf pretrained models [99, 101] and remain frozen during training, requiring no additional supervision. To preserve modality discriminability, we adopt a shared lightweight encoder combined with learnable modality embeddings for unified representation learning. Given the  $m$ -th structural modality input  $x^m$ , the feature extraction process is formulated as:

$$\mathbf{F}^m = E(\phi(x^m) + \mathbf{e}_m), \quad m \in \{\text{Dep}, \text{Seg}, \text{DoG}\}, \quad (7)$$

where  $\phi(\cdot)$  denotes a lightweight input adaptation module, and  $\mathbf{e}_m$  is the corresponding modality embedding. Subsequently, the feature maps are flattened into token sequences:

$$\mathbf{T}^{(m)} = \text{Flat}(\mathbf{F}^m), \quad \mathbf{T}_M = [\mathbf{T}^{(d)}, \mathbf{T}^{(s)}, \mathbf{T}^{(g)}], \quad (8)$$

Since multi-cue structural tokens typically exhibit high redundancy and information overlap, we aim to compress them into a more compact representation. Inspired by [30, 59, 89], we introduce a Structural Token Aggregator (STA) as shown in Figure 3. Specifically, a set of learnable latent tokens  $\mathbf{L} \in \mathbb{R}^{N \times D}$  is employed to actively aggregate essential information from the full set of structural tokens via

cross-attention:

$$\tilde{\mathbf{L}} = \text{CA}(\mathbf{Q} = \mathbf{L}, \mathbf{K} = \mathbf{T}_M, \mathbf{V} = \mathbf{T}_M), \quad (9)$$

Subsequently, linear projection followed by self-attention is applied to enhance token-wise consistency and further reduce inter-modal redundancy, yielding the final structural prior:

$$\mathbf{z}_{\text{struct}} = \text{SA}(\text{Linear}(\tilde{\mathbf{L}})), \quad (10)$$

By jointly leveraging depth, semantic segmentation, and DoG cues, this approach suppresses erroneous edges and spurious artifacts, yielding consistent and coherent geometric representations even under severe degradation. The resulting structural prior provides reliable constraints to guide subsequent restoration.

**Structural Adapter.** The structural prior primarily characterizes the spatial organization and geometric relationships within an image, which is particularly critical for preserving fine-grained structures. To this end, we introduce a Structural Adapter, as shown in Figure 2(c), which injects the structural prior into the shallow layer feature channels of the UNet in a lightweight and parameter-efficient manner, thereby directly constraining local features that are sensitive to structural information. Specifically, the structural tokens are first aggregated into a global structural representation  $\mathbf{s}$  via an aggregation operator  $P(\cdot)$ . Subsequently, a parameterized mapping function  $F(\cdot)$  is employed to predict channel-wise modulation parameters:

$$[\gamma(\mathbf{s}), \beta(\mathbf{s})] = F(P(\mathbf{s})), \quad (11)$$

Given the shallow layer features  $\mathbf{F}_s$ , the structural modulation is formulated as:

$$\mathbf{F}'_s = \mathbf{F}_s \odot (1 + \gamma(\mathbf{s})) + \beta(\mathbf{s}). \quad (12)$$

By modulating features with structural guidance, the Structural Adapter enforces spatial constraints that prevent the loss of fine-grained structural details, mitigating common artifacts like over-smoothing during the denoising process.

### 3.4. Degradation Prior Modeling

**Degradation Prior Learning.** While semantic and structural priors ensure the fidelity and consistency of the restored results, effective restoration under complex degradations still requires accurate degradation information. However, in all-in-one image restoration, since degradation and content cues reside in distinct representational subspaces, their coupling often leads to degradation-content ambiguity, destabilizing degradation awareness and resulting in inaccurate adaptive restoration or residual artifacts in complex scenarios [31]. To address this, we design an independent Degradation Extractor, which learns content-agnostic degradation representations in a dedicated representation subspace, thereby enabling more robust and accurate degradation-aware restoration.

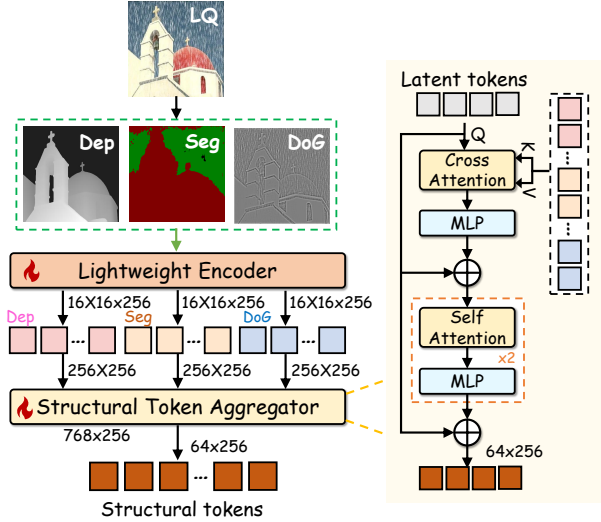


Figure 3. Design of the proposed structural extractor with multi-cue token aggregation. It aggregates heterogeneous tokens to learn unified structural representations for downstream image restoration tasks.

As illustrated in Figure 2(b), given a low-quality input  $x_{\text{LQ}} \in \mathbb{R}^{H \times W \times 3}$ , we employ a pretrained CLIP [72] visual encoder  $E_v$  to extract global features. Leveraging its extensive pretraining on diverse datasets, CLIP provides robust representations that encapsulate rich global semantic and quality-related information.

$$\mathbf{F}_g = E_{\text{deg}}(x_{\text{LQ}}) \in \mathbb{R}^D, \quad (13)$$

Based on these features, we introduce a degradation classifier to perform discriminative supervised learning, which outputs a degradation logits vector  $\mathbf{z}_i \in \mathbb{R}^N$ , where  $N$  denotes the number of predefined degradation categories. During training, we adopt the cross-entropy loss with label smoothing:

$$\mathcal{L}_{\text{deg}} = -\frac{1}{B} \sum_{i=1}^B \sum_{c=1}^N q_{i,c} \log \frac{\exp(z_{i,c})}{\sum_{j=1}^N \exp(z_{i,j})}, \quad (14)$$

where  $q_{i,c} = (1 - \varepsilon) \mathbb{I}[c = y_i] + \varepsilon/N$  with  $\varepsilon = 0.01$ . Here,  $z_{i,c}$  denotes the logit of the  $i$ -th sample for class  $c$ , and  $y_i$  is the corresponding degradation label.

Notably, the degradation classifier is only used during training to guide the model to learn degradation-related discriminative representations. At inference time, the degradation classifier is discarded, and only the continuous features learned by the encoder are retained as the degradation prior  $\mathbf{z}_{\text{deg}}$ , which is subsequently used for conditional modulation in the diffusion-based restoration process.

**Degradation-aware Time Modulation.** Degradation information is typically global in nature and is closely cor-

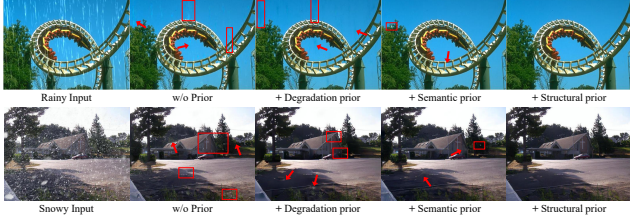


Figure 4. Visual ablation study on prior components. Each prior plays a distinct and indispensable role, where their synergy ensures both geometric integrity and semantic consistency.

related with the noise evolution across the diffusion trajectory. Combining degradation priors with temporal conditions helps the model adaptively adjust its denoising strategy under different noise scales [54]. Therefore, we encode the degradation prior together with the time embedding, allowing it to participate in conditional modulation throughout the entire diffusion trajectory. Specifically, given a diffusion timestep  $\tau$ , its time embedding is defined as:

$$\mathbf{t} = \psi(\tau) \in \mathbb{R}^{D_t}, \quad (15)$$

where  $\psi(\cdot)$  denotes the time embedding mapping function. We project the degradation prior  $\mathbf{z}_{\text{deg}}$  into the time embedding space and modulate it via a learnable temporal adapter:

$$\mathbf{t}' = \mathbf{t} + \phi(\text{softmax}(W_d \mathbf{z}_{\text{deg}}) \odot \mathbf{P}). \quad (16)$$

where  $W_d$  denotes a learnable projection matrix,  $\mathbf{P} \in \mathbb{R}^{D_t}$  is a learnable prompt vector, and  $\phi(\cdot)$  represents a prompt transformation function. This mechanism enables degradation information to be incorporated into temporal conditioning, thereby guiding the model to dynamically adjust its denoising behavior with respect to degradation characteristics across different noise stages.

## 4. Experiments

### 4.1. Experimental Setups

**Datasets.** We considered 9 degradation types in total: low-light enhancement, non-homogeneous dehazing, demoire, deraining, desnowing, dehazing, raindrop removal, defocus deblurring, declouding and denoising. For each degradation type, we collected data from corresponding datasets: Low light: LOL-v1 [93] and LOL-v2 [105]; Non-Homogeneous: NH-HAZE [3]; Moire: RDNet [109]; Rain: Rain100L and Rain200L [103]; Snow: Snow100K-L [51] and WeatherBench [24]; Haze: RESIDE6K [68] and SOTS [37]; Raindrops: Raindrop [67]; Defocus blur: DPDD [1]; Clouds: Recloud [63]; Noise: BSD400 [58], WED [57], and CBSD68 [58]; Motion blur: GoPro [62]. More details are provided in the Appendix.

**Implementation Details.** The proposed method is trained in a two-stage manner. In the first stage, we use

a batch size of 512 with an initial learning rate of  $2 \times 10^{-5}$ . This stage is trained for 30 epochs on a single NVIDIA A100 GPU. In the second stage, the batch size is set to 16, and the input images are randomly cropped to  $256 \times 256$  for data augmentation. The learning rate is fixed at  $2 \times 10^{-5}$ , the diffusion noise level is set to  $\sigma = 50$ , and the number of denoising steps is set to 100. In this stage, we adopt the AdamW [52] optimizer and employ a cosine learning rate decay strategy. Training is conducted on two NVIDIA A100 GPUs for a total of 700K iterations.

**Evaluation Metrics.** To comprehensively evaluate the quantitative performance of different methods, we employ multiple commonly used and widely recognized evaluation metrics. At the pixel level, PSNR and SSIM [91] are employed to measure the fidelity between reconstructed results and reference images. For perceptual quality, FID [4] and LPIPS [118] are respectively utilized to characterize differences in feature distribution distance and perceived similarity between generated results and real images. Additionally, MUSIQ [34] is introduced to evaluate overall image quality.

### 4.2. Comparison with State-of-the-art Methods

**Single-task Image Restoration Results.** We evaluate the proposed method across nine representative single-image restoration tasks. Table 1 summarizes the quantitative comparisons between TPGDiff, task-specific baselines, and state-of-the-art all-in-one restoration approaches. The results demonstrate that TPGDiff consistently achieves superior or competitive performance across the majority of tasks and metrics. This validates the effectiveness of our prior-guided diffusion framework in single-degradation scenarios and underscores its robust generalization across diverse restoration challenges. Comprehensive experimental details are provided in the Appendix.

### Multi-task All-in-one Image Restoration Results.

We further evaluate TPGDiff’s performance in multi-degradation joint training scenarios. Specifically, we select five typical degradation types for joint training and compare them with multiple integrated image restoration methods. As shown in Table 2, TPGDiff achieves optimal or suboptimal results across all quantitative metrics, demonstrating stronger multitask unified modeling capabilities. Further visualization results, as depicted in Figure 5, demonstrate that TPGDiff more stably restores image structure and details across diverse degradation scenarios, exhibiting superior robustness and visual consistency. Additional visualization results and analyses are presented in the appendix.

### 4.3. Ablation study

In this section, we conduct ablation experiments on deraining and desnowing tasks using the Rain200L and Snow100K-L datasets to evaluate the impact of TPGDiff’s individual components on overall performance. All re-

Table 1. Quantitative comparison between our method with other state-of-the-art approaches on nine different degradation-specific datasets.  $\uparrow$  represents the bigger the better, and  $\downarrow$  represents the smaller the better. Best and second-best results are highlighted in **red** and **blue**, respectively.

Method	Low-light Enhancement (LOL-v2)				Method	NH Dehazing (NH-HAZE)				Method	Denoire (RDNet)			
	PSNR $\uparrow$	SSIM $\uparrow$	FID $\downarrow$	LPIPS $\downarrow$		PSNR $\uparrow$	SSIM $\uparrow$	MUSIQ $\uparrow$	LPIPS $\downarrow$		PSNR $\uparrow$	SSIM $\uparrow$	FID $\downarrow$	LPIPS $\downarrow$
Retinexformer [5]	<b>22.80</b>	0.840	62.45	0.169	TransWeather [83]	11.58	0.411	40.22	0.692	SwinIR [45]	24.89	0.888	28.73	0.100
URetinex-Net [97]	19.84	0.824	52.38	0.237	AutoDIR [32]	12.71	0.477	46.29	0.612	RDNet [109]	<b>26.16</b>	<b>0.941</b>	<b>23.64</b>	<b>0.091</b>
Restormer [111]	20.77	0.851	57.04	0.115	DiffUIR [122]	11.39	0.422	47.77	0.651	InsturctIR [17]	24.69	0.843	32.18	0.111
NAFNet [10]	18.04	0.827	54.25	0.147	InstructIR [17]	12.24	<b>0.498</b>	54.80	0.530	UniRestore [8]	24.06	0.819	45.28	0.155
AirNet [38]	19.69	0.821	55.43	0.151	AgenticIR [125]	12.20	0.450	37.47	0.675	FoundIR [43]	24.71	0.876	32.49	0.107
PromptIR [65]	21.23	<b>0.860</b>	53.92	0.145	X-Restormer [15]	11.36	0.413	44.28	0.665	DCPT [28]	24.18	0.815	31.38	0.159
MPeceiver [2]	22.16	0.848	<b>45.90</b>	<b>0.130</b>	FoundIR-v2 [16]	<b>17.00</b>	0.462	<b>65.62</b>	<b>0.334</b>	MaskDCPT [29]	25.21	<b>0.942</b>	24.41	0.095
DA-CLIP [54]	21.76	0.762	48.23	0.134	DA-CLIP [54]	12.35	0.466	49.73	0.590	DA-CLIP [54]	24.75	0.826	38.71	0.134
<b>Ours</b>	<b>24.77</b>	<b>0.880</b>	<b>46.02</b>	<b>0.106</b>	<b>Ours</b>	<b>18.14</b>	<b>0.645</b>	<b>58.43</b>	<b>0.268</b>	<b>Ours</b>	<b>26.40</b>	0.910	<b>22.07</b>	<b>0.089</b>
Method	Deraining (Rain100L)				Method	Desnowing (WeatherBench)				Method	Dehazing (RESIDE)			
	PSNR $\uparrow$	SSIM $\uparrow$	FID $\downarrow$	LPIPS $\downarrow$		PSNR $\uparrow$	SSIM $\uparrow$	MUSIQ $\uparrow$	LPIPS $\downarrow$		PSNR $\uparrow$	SSIM $\uparrow$	FID $\downarrow$	LPIPS $\downarrow$
JORDER [104]	36.61	0.974	14.66	0.028	PromptIR [65]	21.54	0.777	45.20	0.242	GCANet [7]	26.59	0.935	11.52	0.052
PRENET [75]	37.48	0.979	10.98	0.020	TransWeather [83]	20.94	0.758	44.25	0.253	GridDehazeNet [49]	25.86	0.944	10.62	0.048
MAXIM [82]	38.06	0.977	19.06	0.048	DiffUIR [122]	21.68	0.780	45.22	0.240	DehazeFormer [80]	30.29	0.964	7.58	0.045
IR-SDE [55]	38.30	0.981	7.94	0.014	X-Restormer [15]	21.57	<b>0.781</b>	46.04	0.250	MAXIM [82]	29.12	0.932	8.12	0.043
GOUB [108]	<b>39.79</b>	0.983	<b>5.18</b>	<b>0.010</b>	AgenticIR [125]	20.35	0.730	<b>50.87</b>	0.283	IR-SDE [55]	25.25	0.906	8.33	0.060
Perceiver-IR [119]	38.41	<b>0.984</b>	-	-	FoundIR [43]	21.57	0.779	45.72	0.241	AdaIR [19]	<b>30.87</b>	<b>0.975</b>	-	-
VLU-Net [113]	38.60	0.984	-	-	FoundIR-v2 [16]	<b>23.15</b>	0.706	<b>60.15</b>	0.254	DiffRes [86]	30.87	0.970	<b>5.08</b>	<b>0.023</b>
DA-CLIP [54]	37.02	0.978	8.96	0.012	DA-CLIP [54]	21.59	0.773	45.39	<b>0.236</b>	DA-CLIP [54]	30.16	0.936	5.52	0.030
<b>Ours</b>	<b>40.12</b>	<b>0.986</b>	<b>3.47</b>	<b>0.007</b>	<b>Ours</b>	<b>28.17</b>	<b>0.836</b>	50.63	<b>0.104</b>	<b>Ours</b>	<b>32.87</b>	<b>0.979</b>	<b>4.69</b>	<b>0.021</b>
Method	Raindrop Removal (RainDrop)				Method	Defocus Deblur (DPDD)				Method	Declouding (RS-Cloud)			
	PSNR $\uparrow$	SSIM $\uparrow$	FID $\downarrow$	LPIPS $\downarrow$		PSNR $\uparrow$	SSIM $\uparrow$	FID $\downarrow$	LPIPS $\downarrow$		PSNR $\uparrow$	SSIM $\uparrow$	MUSIQ $\uparrow$	LPIPS $\downarrow$
AttGAN [67]	31.59	0.917	22.38	0.058	NRKNet [71]	<b>26.11</b>	<b>0.817</b>	43.96	0.223	PromptIR [65]	11.35	0.772	41.83	0.271
Quanetal [70]	31.37	0.918	30.56	0.065	DRBNet [76]	25.72	0.806	<b>39.37</b>	<b>0.182</b>	DiffUIR [122]	13.82	0.814	38.44	0.260
WeatherDiff [64]	27.06	0.847	49.06	0.089	InsturctIR [17]	23.84	0.746	84.88	0.329	InstructIR [17]	14.46	<b>0.865</b>	<b>47.00</b>	0.163
RDDM [47]	27.07	0.805	51.86	0.102	UniRestore [8]	22.91	0.724	91.59	0.364	X-Restormer [15]	11.48	0.751	35.99	0.325
DiffUIR [122]	26.88	0.817	55.84	0.114	FoundIR [43]	23.45	0.742	89.21	0.358	AgenticIR [125]	17.80	0.799	34.90	0.257
DiffRes [86]	<b>33.70</b>	<b>0.939</b>	<b>19.65</b>	<b>0.047</b>	DCPT [28]	25.68	0.816	42.59	0.216	FoundIR [43]	11.71	0.753	35.40	0.322
IRBridge [87]	26.91	0.813	49.15	0.098	MaskDCPT [29]	25.64	0.809	<b>38.49</b>	0.183	FoundIR-v2 [16]	<b>22.06</b>	0.828	<b>44.37</b>	<b>0.125</b>
DA-CLIP [54]	30.75	0.892	24.31	0.061	DA-CLIP [54]	23.55	0.747	67.54	0.288	DA-CLIP [54]	16.43	0.803	35.73	0.238
<b>Ours</b>	<b>32.29</b>	<b>0.923</b>	<b>19.16</b>	<b>0.046</b>	<b>Ours</b>	<b>26.85</b>	<b>0.816</b>	42.04	<b>0.144</b>	<b>Ours</b>	<b>38.37</b>	<b>0.954</b>	42.97	<b>0.037</b>

Table 2. Quantitative comparison between our method and other state-of-the-art approaches on five restoration tasks.  $\uparrow$  represents the bigger the better. Best and second-best results are highlighted in **red** and **blue**, respectively.

Method	Low-light		Deblurring		Deraining		Dehazing		Denoising		Average	
	PSNR $\uparrow$	SSIM $\uparrow$										
AirNet [38]	18.18	0.735	24.35	0.781	32.98	0.951	21.04	0.884	30.91	0.882	25.49	0.846
IR-SDE [55]	20.07	0.780	26.34	0.800	34.12	0.951	24.56	0.940	30.89	0.865	27.20	0.867
PromptIR [65]	22.89	0.829	<b>27.93</b>	<b>0.851</b>	36.17	0.970	30.41	0.972	31.20	0.885	29.72	0.901
DA-CLIP [54]	21.66	0.828	27.31	0.838	35.65	0.962	29.78	0.968	30.93	0.885	29.07	0.896
DiffUIR [122]	22.32	0.826	27.50	0.845	35.98	0.968	29.47	0.965	31.02	0.885	29.25	0.898
InstructIR [17]	20.70	0.820	26.65	0.810	35.58	0.967	25.20	0.938	31.09	0.883	27.84	0.884
FoundIR [43]	12.81	0.642	25.87	0.801	29.39	0.918	19.74	0.878	24.45	0.637	22.45	0.775
DCPT [28]	20.38	0.836	26.42	0.807	35.70	0.974	28.67	0.973	31.16	0.882	28.47	0.894
PoolNet [18]	22.66	0.841	27.66	0.844	37.85	<b>0.981</b>	30.25	0.977	<b>31.24</b>	<b>0.887</b>	29.93	<b>0.906</b>
TUR_AirNet [95]	17.88	0.772	26.13	0.801	33.95	0.962	27.59	0.954	30.93	0.875	27.30	0.873
VLU-Net [113]	<b>23.00</b>	<b>0.852</b>	27.46	0.840	<b>38.54</b>	0.982	30.84	<b>0.980</b>	<b>31.43</b>	<b>0.891</b>	<b>30.11</b>	0.905
<b>Ours</b>	<b>24.52</b>	<b>0.857</b>	<b>28.94</b>	<b>0.863</b>	<b>38.05</b>	<b>0.982</b>	<b>30.90</b>	<b>0.987</b>	30.58	0.853	<b>30.60</b>	<b>0.908</b>

ported metrics represent the average results across both tasks.

**Effectiveness of Different Types of Priors.** To evaluate the contribution of each prior, we conduct a progres-

sive ablation study, as reported in Table 3. Starting from the baseline, the incorporation of degradation and semantic priors leads to improvements in both pixel-level accuracy and perceptual quality. With the further introduction of the

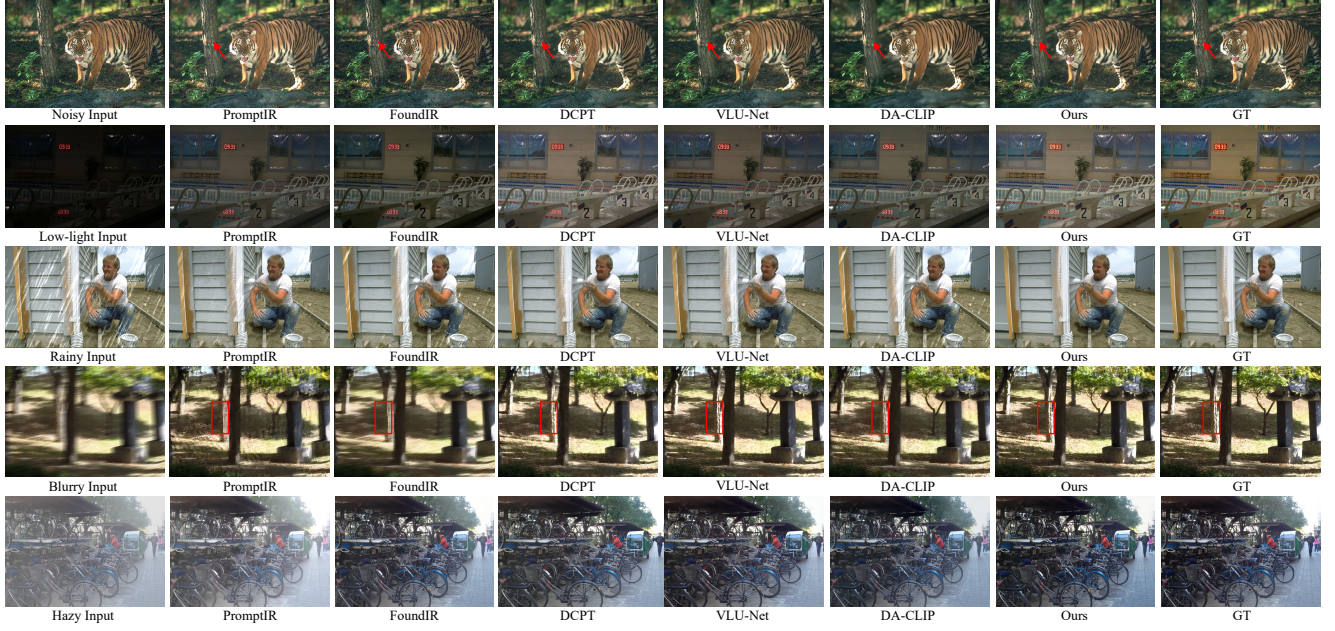


Figure 5. Visual comparison results and other all-in-one image restoration methods on image denoising, low-light enhancement, image deraining, and image deblurring tasks. Zoom in for a better view.

Table 3. **Ablation study on prior types.** We evaluate the impact of different prior types on guiding the recovery process.

Model	Method			Metrics		
	Deg.	Sem.	Struc.	PSNR $\uparrow$	SSIM $\uparrow$	LPIPS $\downarrow$
(a)	$\times$	$\times$	$\times$	31.63	0.912	0.060
(b)	$\checkmark$	$\times$	$\times$	31.93	0.912	0.060
(c)	$\checkmark$	$\checkmark$	$\times$	32.61	0.920	0.049
Ours	$\checkmark$	$\checkmark$	$\checkmark$	32.63	0.921	0.045

Table 4. **Ablation study on input positions.** We compare the four combinations of injecting semantic and structural priors at deep versus shallow layers.

Semantic Prior		Structural Prior		Metrics		
Deep	Shallow	Deep	Shallow	PSNR $\uparrow$	SSIM $\uparrow$	LPIPS $\downarrow$
$\checkmark$	$\checkmark$	$\times$	$\times$	32.38	0.918	0.051
$\times$	$\checkmark$	$\checkmark$	$\times$	32.18	0.915	0.052
$\checkmark$	$\times$	$\times$	$\checkmark$	32.63	0.921	0.045

structural prior, all evaluation metrics are consistently optimized. The visual comparisons in Figure 4 confirm the necessity and synergy of each prior component.

**Effectiveness of Prior Input Positions.** To further investigate the sensitivity differences of diffusion model layers to various priors, we conduct an alignment study on prior injection positions. As shown in Table 4, the model

achieves optimal performance when semantic priors are applied to deep layers and structural priors are injected into shallow layers.

## 5. Conclusion

In this paper, we presented TPGDiff, a novel Triple-Prior Guided Diffusion framework designed for unified image restoration. The core of our approach lies in the hierarchical and complementary coordination of multi-faceted priors. By integrating multi-source structural cues into shallow layers and distillation-driven semantic priors into deep layers, TPGDiff successfully bridges the gap between geometric precision and contextual plausibility. Furthermore, the inclusion of degradation-aware priors ensures stage-adaptive guidance throughout the entire diffusion trajectory. Extensive evaluations confirm that our tri-prior integration effectively mitigates structural distortion and semantic drift, setting a new benchmark for robustness and fidelity in all-in-one restoration tasks.

## References

- [1] Abdullah Abuolaim and Michael S Brown. Defocus deblurring using dual-pixel data. In *European conference on computer vision*, pages 111–126. Springer, 2020. 6, 16
- [2] Yuang Ai, Huabo Huang, Xiaoqiang Zhou, Jieyang Wang, and Ran He. Multimodal prompt perceiver: Empower adaptiveness generalizability and fidelity for all-in-one image restoration. In *Proceedings of the IEEE/CVF Conference*

*on Computer Vision and Pattern Recognition*, pages 25432–25444, 2024. 1, 2, 7

[3] Codruta O Ancuti, Cosmin Ancuti, and Radu Timofte. Nh-haze: An image dehazing benchmark with non-homogeneous hazy and haze-free images. In *Proceedings of the IEEE/CVF conference on computer vision and pattern recognition workshops*, pages 444–445, 2020. 6, 16

[4] Naresh Babu Bynagari. Gans trained by a two time-scale update rule converge to a local nash equilibrium. *Asian Journal of Applied Science and Engineering*, 8(1):25–34, 2019. 6

[5] Yuanhao Cai, Hao Bian, Jing Lin, Haoqian Wang, Radu Timofte, and Yulun Zhang. Retinexformer: One-stage retinex-based transformer for low-light image enhancement. In *Proceedings of the IEEE/CVF international conference on computer vision*, pages 12504–12513, 2023. 7

[6] Shuo Cao, Yihao Liu, Wenlong Zhang, Yu Qiao, and Chao Dong. Grids: Grouped multiple-degradation restoration with image degradation similarity. In *European Conference on Computer Vision*, pages 70–87. Springer, 2024. 2

[7] Dongdong Chen, Mingming He, Qingnan Fan, Jing Liao, Liheng Zhang, Dongdong Hou, Lu Yuan, and Gang Hua. Gated context aggregation network for image dehazing and deraining. In *2019 IEEE winter conference on applications of computer vision (WACV)*, pages 1375–1383. IEEE, 2019. 7

[8] I Chen, Wei-Ting Chen, Yu-Wei Liu, Yuan-Chun Chiang, Sy-Yen Kuo, Ming-Hsuan Yang, et al. Unirestore: Unified perceptual and task-oriented image restoration model using diffusion prior. In *Proceedings of the Computer Vision and Pattern Recognition Conference*, pages 17969–17979, 2025. 7

[9] Liangyu Chen, Xin Lu, Jie Zhang, Xiaojie Chu, and Cheng-peng Chen. Hinet: Half instance normalization network for image restoration. In *Proceedings of the IEEE/CVF conference on computer vision and pattern recognition*, pages 182–192, 2021. 18

[10] Liangyu Chen, Xiaojie Chu, Xiangyu Zhang, and Jian Sun. Simple baselines for image restoration. In *European conference on computer vision*, pages 17–33. Springer, 2022. 1, 7, 18

[11] Sixiang Chen, Tian Ye, Jinbin Bai, Erkang Chen, Jun Shi, and Lei Zhu. Sparse sampling transformer with uncertainty-driven ranking for unified removal of raindrops and rain streaks. In *Proceedings of the IEEE/CVF international conference on computer vision*, pages 13106–13117, 2023. 1

[12] Wei-Ting Chen, Hao-Yu Fang, Jian-Jiun Ding, Cheng-Che Tsai, and Sy-Yen Kuo. Jstasr: Joint size and transparency-aware snow removal algorithm based on modified partial convolution and veiling effect removal. In *European conference on computer vision*, pages 754–770. Springer, 2020. 1

[13] Wei-Ting Chen, Hao-Yu Fang, Cheng-Lin Hsieh, Cheng-Che Tsai, I Chen, Jian-Jiun Ding, Sy-Yen Kuo, et al. All snow removed: Single image desnowing algorithm using hierarchical dual-tree complex wavelet representation and contradict channel loss. In *Proceedings of the IEEE/CVF international conference on computer vision*, pages 4196–4205, 2021. 1

[14] Xiang Chen, Hao Li, Mingqiang Li, and Jinshan Pan. Learning a sparse transformer network for effective image deraining. In *Proceedings of the IEEE/CVF conference on computer vision and pattern recognition*, pages 5896–5905, 2023. 1

[15] Xiangyu Chen, Zheyuan Li, Yuandong Pu, Yihao Liu, Jiantao Zhou, Yu Qiao, and Chao Dong. A comparative study of image restoration networks for general backbone network design. In *European Conference on Computer Vision*, pages 74–91. Springer, 2024. 7

[16] Xiang Chen, Jinshan Pan, Jiangxin Dong, Jian Yang, and Jinhui Tang. Foundir-v2: Optimizing pre-training data mixtures for image restoration foundation model. *arXiv preprint arXiv:2512.09282*, 2025. 7

[17] Marcos V Conde, Gregor Geigle, and Radu Timofte. Instructir: High-quality image restoration following human instructions. In *European Conference on Computer Vision*, pages 1–21. Springer, 2024. 7

[18] Yuning Cui, Wenqi Ren, and Alois Knoll. Exploring the potential of pooling techniques for universal image restoration. *IEEE Transactions on Image Processing*, 2025. 7

[19] Yuning Cui, Syed Waqas Zamir, Salman Khan, Alois Knoll, Mubarak Shah, and Fahad Shahbaz Khan. Adair: Adaptive all-in-one image restoration via frequency mining and modulation. In *13th international conference on learning representations, ICLR 2025*, pages 57335–57356. International Conference on Learning Representations, ICLR, 2025. 7

[20] Xin Deng, Chenxiao Zhang, Lai Jiang, Jingyuan Xia, and Mai Xu. Deepsn-net: Deep semi-smooth newton driven network for blind image restoration. *IEEE Transactions on Pattern Analysis and Machine Intelligence*, 2025. 18

[21] Zheng Ding, Xuaner Zhang, Zhuowen Tu, and Zhihao Xia. Restoration by generation with constrained priors. In *Proceedings of the IEEE/CVF Conference on Computer Vision and Pattern Recognition*, pages 2567–2577, 2024. 2

[22] Qingnan Fan, Dongdong Chen, Lu Yuan, Gang Hua, Nenghai Yu, and Baoquan Chen. A general decoupled learning framework for parameterized image operators. *IEEE transactions on pattern analysis and machine intelligence*, 43(1):33–47, 2019. 18

[23] Jiayi Fu, Siyu Liu, Zikun Liu, Chun-Le Guo, Hyunhee Park, Ruiqi Wu, Guoqing Wang, and Chongyi Li. Iterative predictor-critic code decoding for real-world image dehazing. In *Proceedings of the Computer Vision and Pattern Recognition Conference*, pages 12700–12709, 2025. 1

[24] Qiyuan Guan, Qianfeng Yang, Xiang Chen, Tianyu Song, Guiyue Jin, and Jiyu Jin. Weatherbench: A real-world benchmark dataset for all-in-one adverse weather image restoration. In *Proceedings of the 33rd ACM international conference on multimedia*, pages 12607–12613, 2025. 6, 16

[25] Chun-Le Guo, Qixin Yan, Saeed Anwar, Runmin Cong, Wenqi Ren, and Chongyi Li. Image dehazing transformer with transmission-aware 3d position embedding. In *Proceedings of the IEEE/CVF conference on computer vision and pattern recognition*, pages 5812–5820, 2022. 1

[26] Yu Guo, Yuan Gao, Yuxu Lu, Huilin Zhu, Ryan Wen Liu, and Shengfeng He. Onerestore: A universal restoration framework for composite degradation. In *European conference on computer vision*, pages 255–272. Springer, 2024. 2

[27] Jonathan Ho, Ajay Jain, and Pieter Abbeel. Denoising diffusion probabilistic models. *Advances in neural information processing systems*, 33:6840–6851, 2020. 2

[28] JiaKui Hu, Lujia Jin, Zhengjian Yao, and Yanye Lu. Universal image restoration pre-training via degradation classification. *arXiv preprint arXiv:2501.15510*, 2025. 1, 7

[29] JiaKui Hu, Zhengjian Yao, Lujia Jin, Yinghao Chen, and Yanye Lu. Universal image restoration pre-training via masked degradation classification. *arXiv preprint arXiv:2510.13282*, 2025. 2, 7

[30] Andrew Jaegle, Felix Gimeno, Andy Brock, Oriol Vinyals, Andrew Zisserman, and Joao Carreira. Perceiver: General perception with iterative attention. In *International conference on machine learning*, pages 4651–4664. PMLR, 2021. 4

[31] Junjun Jiang, Zengyuan Zuo, Gang Wu, Kui Jiang, and Xianming Liu. A survey on all-in-one image restoration: Taxonomy, evaluation and future trends. *IEEE Transactions on Pattern Analysis and Machine Intelligence*, 2025. 5

[32] Yitong Jiang, Zhaoyang Zhang, Tianfan Xue, and Jinwei Gu. Autodir: Automatic all-in-one image restoration with latent diffusion. In *European Conference on Computer Vision*, pages 340–359. Springer, 2024. 7

[33] Xin Jin, Ling-Hao Han, Zhen Li, Chun-Le Guo, Zhi Chai, and Chongyi Li. Dnf: Decouple and feedback network for seeing in the dark. In *Proceedings of the IEEE/CVF conference on computer vision and pattern recognition*, pages 18135–18144, 2023. 1

[34] Junjie Ke, Qifei Wang, Yilin Wang, Peyman Milanfar, and Feng Yang. Musiq: Multi-scale image quality transformer. In *Proceedings of the IEEE/CVF international conference on computer vision*, pages 5148–5157, 2021. 6

[35] Dehong Kong, Fan Li, Zhixin Wang, Jiaqi Xu, Renjing Pei, Wenbo Li, and WenQi Ren. Dual prompting image restoration with diffusion transformers. In *Proceedings of the Computer Vision and Pattern Recognition Conference*, pages 12809–12819, 2025. 2

[36] Xiangtao Kong, Chao Dong, and Lei Zhang. Towards effective multiple-in-one image restoration: A sequential and prompt learning strategy. *arXiv preprint arXiv:2401.03379*, 2024. 2

[37] Boyi Li, Wenqi Ren, Dengpan Fu, Dacheng Tao, Dan Feng, Wenjun Zeng, and Zhangyang Wang. Benchmarking single-image dehazing and beyond. *IEEE transactions on image processing*, 28(1):492–505, 2018. 6, 16

[38] Boyun Li, Xiao Liu, Peng Hu, Zhongqin Wu, Jiancheng Lv, and Xi Peng. All-in-one image restoration for unknown corruption. In *Proceedings of the IEEE/CVF conference on computer vision and pattern recognition*, pages 17452–17462, 2022. 1, 2, 7, 18

[39] Bingchen Li, Xin Li, Yiting Lu, Ruoyu Feng, Mengxi Guo, Shijie Zhao, Li Zhang, and Zhibo Chen. Promptcir: Blind compressed image restoration with prompt learning. In *Proceedings of the IEEE/CVF Conference on Computer Vision and Pattern Recognition*, pages 6442–6452, 2024. 1

[40] Boyun Li, Haiyu Zhao, Wenxin Wang, Peng Hu, Yuanbiao Gou, and Xi Peng. Mair: A locality-and continuity-preserving mamba for image restoration. In *Proceedings of the Computer Vision and Pattern Recognition Conference*, pages 7491–7501, 2025. 18

[41] Chongyi Li, Chun-Le Guo, Man Zhou, Zhixin Liang, Shangchen Zhou, Ruicheng Feng, and Chen Change Loy. Embedding fourier for ultra-high-definition low-light image enhancement. *arXiv preprint arXiv:2302.11831*, 2023. 1

[42] Dong Li, Yidi Liu, Xueyang Fu, Senyan Xu, and Zheng-Jun Zha. Fouriermamba: Fourier learning integration with state space models for image deraining. *arXiv preprint arXiv:2405.19450*, 2024. 1

[43] Hao Li, Xiang Chen, Jiangxin Dong, Jinhui Tang, and Jinshan Pan. Foundir: Unleashing million-scale training data to advance foundation models for image restoration. In *Proceedings of the IEEE/CVF international conference on computer vision*, pages 12626–12636, 2025. 2, 7

[44] Xinrui Li, Jianlong Wu, Xinchuan Huang, Chong Chen, Weili Guan, Xian-Sheng Hua, and Liqiang Nie. Megasr: Mining customized semantics and expressive guidance for image super-resolution. *arXiv preprint arXiv:2503.08096*, 2025. 2

[45] Jingyun Liang, Jiezheng Cao, Guolei Sun, Kai Zhang, Luc Van Gool, and Radu Timofte. Swinir: Image restoration using swin transformer. In *Proceedings of the IEEE/CVF international conference on computer vision*, pages 1833–1844, 2021. 7, 18

[46] Xin Lin, Chao Ren, Xiao Liu, Jie Huang, and Yinjie Lei. Unsupervised image denoising in real-world scenarios via self-collaboration parallel generative adversarial branches. In *Proceedings of the IEEE/CVF International Conference on Computer Vision*, pages 12642–12652, 2023. 1

[47] Jiawei Liu, Qiang Wang, Huijie Fan, Yinong Wang, Yandong Tang, and Liangqiong Qu. Residual denoising diffusion models. In *Proceedings of the IEEE/CVF Conference on Computer Vision and Pattern Recognition*, pages 2773–2783, 2024. 7, 18

[48] Lin Liu, Lingxi Xie, Xiaopeng Zhang, Shanxin Yuan, Xiangyu Chen, Wengang Zhou, Houqiang Li, and Qi Tian. Tape: Task-agnostic prior embedding for image restoration. In *European conference on computer vision*, pages 447–464. Springer, 2022. 18

[49] Xiaohong Liu, Yongrui Ma, Zhihao Shi, and Jun Chen. Griddehazenet: Attention-based multi-scale network for image dehazing. In *Proceedings of the IEEE/CVF international conference on computer vision*, pages 7314–7323, 2019. 7

[50] Yuhao Liu, Zhanghan Ke, Fang Liu, Nanxuan Zhao, and Rynson WH Lau. Diff-plugin: Revitalizing details for diffusion-based low-level tasks. In *Proceedings of the IEEE/CVF Conference on Computer Vision and Pattern Recognition*, pages 4197–4208, 2024. 3

[51] Yun-Fu Liu, Da-Wei Jaw, Shih-Chia Huang, and Jenq-Neng Hwang. Desnownet: Context-aware deep network for snow removal. *IEEE Transactions on Image Processing*, 27(6):3064–3073, 2018. 1, 6

[52] Ilya Loshchilov and Frank Hutter. Decoupled weight decay regularization. *arXiv preprint arXiv:1711.05101*, 2017. 6

[53] Wenyang Luo, Haina Qin, Zewen Chen, Libin Wang, Dandan Zheng, Yuming Li, Yufan Liu, Bing Li, and Weiming Hu. Visual-instructed degradation diffusion for all-in-one image restoration. In *Proceedings of the Computer Vision and Pattern Recognition Conference*, pages 12764–12777, 2025. 1

[54] Ziwei Luo, Fredrik K Gustafsson, Zheng Zhao, Jens Sjölund, and Thomas B Schön. Controlling vision-language models for universal image restoration. *arXiv preprint arXiv:2310.01018*, 3(8), 2023. 2, 3, 6, 7, 18

[55] Ziwei Luo, Fredrik K Gustafsson, Zheng Zhao, Jens Sjölund, and Thomas B Schön. Image restoration with mean-reverting stochastic differential equations. *arXiv preprint arXiv:2301.11699*, 2023. 3, 7, 15

[56] Jiaqi Ma, Tianheng Cheng, Guoli Wang, Qian Zhang, Xinggang Wang, and Lefei Zhang. Prores: Exploring degradation-aware visual prompt for universal image restoration. *arXiv preprint arXiv:2306.13653*, 2023. 2

[57] Kede Ma, Zhengfang Duanmu, Qingbo Wu, Zhou Wang, Hongwei Yong, Hongliang Li, and Lei Zhang. Waterloo exploration database: New challenges for image quality assessment models. *IEEE Transactions on Image Processing*, 26(2):1004–1016, 2016. 6, 16

[58] David Martin, Charless Fowlkes, Doron Tal, and Jitendra Malik. A database of human segmented natural images and its application to evaluating segmentation algorithms and measuring ecological statistics. In *Proceedings eighth IEEE international conference on computer vision. ICCV 2001*, pages 416–423. IEEE, 2001. 6, 16

[59] Kangfu Mei, Hossein Talebi, Mojtaba Ardakani, Vishal M Patel, Peyman Milanfar, and Mauricio Delbracio. The power of context: How multimodality improves image super-resolution. In *Proceedings of the Computer Vision and Pattern Recognition Conference*, pages 23141–23152, 2025. 2, 4

[60] Chong Mou, Qian Wang, and Jian Zhang. Deep generalized unfolding networks for image restoration. In *Proceedings of the IEEE/CVF conference on computer vision and pattern recognition*, pages 17399–17410, 2022. 18

[61] Chong Mou, Xiantao Wang, Liangbin Xie, Yanze Wu, Jian Zhang, Zhongang Qi, and Ying Shan. T2i-adapter: Learning adapters to dig out more controllable ability for text-to-image diffusion models. In *Proceedings of the AAAI conference on artificial intelligence*, pages 4296–4304, 2024. 2

[62] Seungjun Nah, Tae Hyun Kim, and Kyoung Mu Lee. Deep multi-scale convolutional neural network for dynamic scene deblurring. In *Proceedings of the IEEE conference on computer vision and pattern recognition*, pages 3883–3891, 2017. 6, 16

[63] Jin Ning, Lianbin Xie, Jie Yin, and Yiguang Liu. Cloud removal advances: A comprehensive review and analysis for optical remote sensing images. *IEEE Journal of Selected Topics in Applied Earth Observations and Remote Sensing*, 2025. 6, 16

[64] Ozan Özdenizci and Robert Legenstein. Restoring vision in adverse weather conditions with patch-based denoising diffusion models. *IEEE transactions on pattern analysis and machine intelligence*, 45(8):10346–10357, 2023. 7

[65] Vaishnav Potlapalli, Syed Waqas Zamir, Salman H Khan, and Fahad Shahbaz Khan. Promptir: Prompting for all-in-one image restoration. *Advances in Neural Information Processing Systems*, 36:71275–71293, 2023. 1, 2, 7

[66] Chenyang Qi, Zhengzhong Tu, Keren Ye, Mauricio Delbracio, Peyman Milanfar, Qifeng Chen, and Hossein Talebi. Spire: Semantic prompt-driven image restoration. In *European Conference on Computer Vision*, pages 446–464. Springer, 2024. 2

[67] Rui Qian, Robby T Tan, Wenhan Yang, Jiajun Su, and Jiaying Liu. Attentive generative adversarial network for raindrop removal from a single image. In *Proceedings of the IEEE conference on computer vision and pattern recognition*, pages 2482–2491, 2018. 6, 7, 16

[68] Xu Qin, Zhilin Wang, Yuanchao Bai, Xiaodong Xie, and Huizhu Jia. Ffa-net: Feature fusion attention network for single image dehazing. In *Proceedings of the AAAI conference on artificial intelligence*, pages 11908–11915, 2020. 6, 16

[69] Yunpeng Qu, Kun Yuan, Kai Zhao, Qizhi Xie, Jinhua Hao, Ming Sun, and Chao Zhou. Xpsr: Cross-modal priors for diffusion-based image super-resolution. In *European Conference on Computer Vision*, pages 285–303. Springer, 2024. 2

[70] Yuhui Quan, Shijie Deng, Yixin Chen, and Hui Ji. Deep learning for seeing through window with raindrops. In *Proceedings of the IEEE/CVF international conference on computer vision*, pages 2463–2471, 2019. 7

[71] Yuhui Quan, Zicong Wu, and Hui Ji. Neumann network with recursive kernels for single image defocus deblurring. In *Proceedings of the IEEE/CVF conference on computer vision and pattern recognition*, pages 5754–5763, 2023. 1, 7

[72] Alec Radford, Jong Wook Kim, Chris Hallacy, Aditya Ramesh, Gabriel Goh, Sandhini Agarwal, Girish Sastry, Amanda Askell, Pamela Mishkin, Jack Clark, et al. Learning transferable visual models from natural language supervision. In *International conference on machine learning*, pages 8748–8763. PMLR, 2021. 4, 5

[73] Sudarshan Rajagopalan and Vishal M Patel. Awracle: All-weather image restoration using visual in-context learning. In *Proceedings of the AAAI Conference on Artificial Intelligence*, pages 6675–6683, 2025. 18

[74] Aditya Ramesh, Prafulla Dhariwal, Alex Nichol, Casey Chu, and Mark Chen. Hierarchical text-conditional image generation with clip latents. *arXiv preprint arXiv:2204.06125*, 1(2):3, 2022. 2

[75] Dongwei Ren, Wangmeng Zuo, Qinghua Hu, Pengfei Zhu, and Deyu Meng. Progressive image deraining networks: A better and simpler baseline. In *Proceedings of*

*the IEEE/CVF conference on computer vision and pattern recognition*, pages 3937–3946, 2019. 7

[76] Lingyan Ruan, Bin Chen, Jizhou Li, and Miuling Lam. Learning to deblur using light field generated and real defocus images. In *Proceedings of the IEEE/CVF conference on computer vision and pattern recognition*, pages 16304–16313, 2022. 7

[77] Chitwan Saharia, William Chan, Saurabh Saxena, Lala Li, Jay Whang, Emily L Denton, Kamyar Ghasemipour, Raphael Gontijo Lopes, Burcu Karagol Ayan, Tim Salimans, et al. Photorealistic text-to-image diffusion models with deep language understanding. *Advances in neural information processing systems*, 35:36479–36494, 2022. 2

[78] Kai Shang, Mingwen Shao, Chao Wang, Yuanshuo Cheng, and Shuigen Wang. Multi-domain multi-scale diffusion model for low-light image enhancement. In *Proceedings of the AAAI conference on artificial intelligence*, pages 4722–4730, 2024. 1

[79] Yang Song, Jascha Sohl-Dickstein, Diederik P Kingma, Abhishek Kumar, Stefano Ermon, and Ben Poole. Score-based generative modeling through stochastic differential equations. *arXiv preprint arXiv:2011.13456*, 2020. 2, 15

[80] Yuda Song, Zhuqing He, Hui Qian, and Xin Du. Vision transformers for single image dehazing. *IEEE Transactions on Image Processing*, 32:1927–1941, 2023. 1, 7

[81] Fu-Jen Tsai, Yan-Tsung Peng, Yen-Yu Lin, Chung-Chi Tsai, and Chia-Wen Lin. Stripformer: Strip transformer for fast image deblurring. In *European conference on computer vision*, pages 146–162. Springer, 2022. 1

[82] Zhengzhong Tu, Hossein Talebi, Han Zhang, Feng Yang, Peyman Milanfar, Alan Bovik, and Yinxiao Li. Maxim: Multi-axis mlp for image processing. In *Proceedings of the IEEE/CVF conference on computer vision and pattern recognition*, pages 5769–5780, 2022. 7

[83] Jeya Maria Jose Valanarasu, Rajeev Yasarla, and Vishal M Patel. Transweather: Transformer-based restoration of images degraded by adverse weather conditions. In *Proceedings of the IEEE/CVF conference on computer vision and pattern recognition*, pages 2353–2363, 2022. 1, 7

[84] Andrey Voynov, Qinghao Chu, Daniel Cohen-Or, and Kfir Aberman. p+: Extended textual conditioning in text-to-image generation. *arXiv preprint arXiv:2303.09522*, 2023. 2

[85] Cong Wang, Jinshan Pan, Wei Wang, Jiangxin Dong, Mengzhu Wang, Yakun Ju, and Junyang Chen. Promptre-storer: A prompting image restoration method with degradation perception. *Advances in Neural Information Processing Systems*, 36:8898–8912, 2023. 1

[86] Chao Wang, Hehe Fan, Huichen Yang, Sarvnaz Karimi, Lina Yao, and Yi Yang. Adapting text-to-image generation with feature difference instruction for generic image restoration. In *Proceedings of the Computer Vision and Pattern Recognition Conference*, pages 23539–23550, 2025. 1, 2, 3, 7

[87] Hanting Wang, Tao Jin, Wang Lin, Shulei Wang, Hai Huang, Shengpeng Ji, and Zhou Zhao. Irbridge: Solving image restoration bridge with pre-trained generative diffusion models. *arXiv preprint arXiv:2505.24406*, 2025. 2, 7

[88] Hebaixu Wang, Jing Zhang, Haoyang Chen, Haonan Guo, Di Wang, Jiayi Ma, and Bo Du. Residual diffusion bridge model for image restoration. *arXiv preprint arXiv:2510.23116*, 2025. 1

[89] Sinong Wang, Belinda Z Li, Madian Khabsa, Han Fang, and Hao Ma. Linformer: Self-attention with linear complexity. *arXiv preprint arXiv:2006.04768*, 2020. 4

[90] Yongzhen Wang, Xuefeng Yan, Fu Lee Wang, Haoran Xie, Wenhan Yang, Xiao-Ping Zhang, Jing Qin, and Mingqiang Wei. Ucl-dehaze: Toward real-world image dehazing via unsupervised contrastive learning. *IEEE Transactions on Image Processing*, 33:1361–1374, 2024. 1

[91] Zhou Wang, Alan C Bovik, Hamid R Sheikh, and Eero P Simoncelli. Image quality assessment: from error visibility to structural similarity. *IEEE transactions on image processing*, 13(4):600–612, 2004. 6

[92] Zichun Wang, Ying Fu, Ji Liu, and Yulun Zhang. Lg-bpn: Local and global blind-patch network for self-supervised real-world denoising. In *Proceedings of the IEEE/CVF conference on computer vision and pattern recognition*, pages 18156–18165, 2023. 1

[93] Chen Wei, Wenjing Wang, Wenhan Yang, and Jiaying Liu. Deep retinex decomposition for low-light enhancement. *arXiv preprint arXiv:1808.04560*, 2018. 6, 16

[94] Hongyang Wei, Shuaizheng Liu, Chun Yuan, and Lei Zhang. Perceive, understand and restore: Real-world image super-resolution with autoregressive multimodal generative models. *arXiv preprint arXiv:2503.11073*, 2025. 2

[95] Gang Wu, Junjun Jiang, Yijun Wang, Kui Jiang, and Xianming Liu. Debiased all-in-one image restoration with task uncertainty regularization. In *Proceedings of the AAAI Conference on Artificial Intelligence*, pages 8386–8394, 2025. 7

[96] Rongyuan Wu, Tao Yang, Lingchen Sun, Zhengqiang Zhang, Shuai Li, and Lei Zhang. Seesr: Towards semantics-aware real-world image super-resolution. In *Proceedings of the IEEE/CVF conference on computer vision and pattern recognition*, pages 25456–25467, 2024. 2

[97] Wenhui Wu, Jian Weng, Pingping Zhang, Xu Wang, Wenhan Yang, and Jianmin Jiang. Uretinex-net: Retinex-based deep unfolding network for low-light image enhancement. In *Proceedings of the IEEE/CVF conference on computer vision and pattern recognition*, pages 5901–5910, 2022. 7

[98] Yuhui Wu, Chen Pan, Guoqing Wang, Yang Yang, Jiwei Wei, Chongyi Li, and Heng Tao Shen. Learning semantic-aware knowledge guidance for low-light image enhancement. In *Proceedings of the IEEE/CVF conference on computer vision and pattern recognition*, pages 1662–1671, 2023. 1

[99] Enze Xie, Wenhui Wang, Zhiding Yu, Anima Anandkumar, Jose M Alvarez, and Ping Luo. Segformer: Simple and efficient design for semantic segmentation with transformers. *Advances in neural information processing systems*, 34:12077–12090, 2021. 4

[100] Xiaogang Xu, Ruixing Wang, and Jiangbo Lu. Low-light image enhancement via structure modeling and guidance.

In *Proceedings of the IEEE/CVF conference on computer vision and pattern recognition*, pages 9893–9903, 2023. 1

[101] Honghui Yang, Di Huang, Wei Yin, Chunhua Shen, Haifeng Liu, Xiaofei He, Binbin Lin, Wanli Ouyang, and Tong He. Depth any video with scalable synthetic data. *arXiv preprint arXiv:2410.10815*, 2024. 4

[102] Tao Yang, Rongyuan Wu, Peiran Ren, Xuansong Xie, and Lei Zhang. Pixel-aware stable diffusion for realistic image super-resolution and personalized stylization. In *European conference on computer vision*, pages 74–91. Springer, 2024. 2

[103] Wenhan Yang, Robby T Tan, Jiashi Feng, Jiaying Liu, Zongming Guo, and Shuicheng Yan. Deep joint rain detection and removal from a single image. In *Proceedings of the IEEE conference on computer vision and pattern recognition*, pages 1357–1366, 2017. 6, 16

[104] Wenhan Yang, Robby T Tan, Jiashi Feng, Zongming Guo, Shuicheng Yan, and Jiaying Liu. Joint rain detection and removal from a single image with contextualized deep networks. *IEEE transactions on pattern analysis and machine intelligence*, 42(6):1377–1393, 2019. 7

[105] Wenhan Yang, Wenjing Wang, Haofeng Huang, Shiqi Wang, and Jiaying Liu. Sparse gradient regularized deep retinex network for robust low-light image enhancement. *IEEE Transactions on Image Processing*, 30:2072–2086, 2021. 6, 16

[106] Mingde Yao, Ruikang Xu, Yuanshen Guan, Jie Huang, and Zhiwei Xiong. Neural degradation representation learning for all-in-one image restoration. *IEEE transactions on image processing*, 2024. 1

[107] Tian Ye, Sixiang Chen, Wenhao Chai, Zhaohu Xing, Jing Qin, Ge Lin, and Lei Zhu. Learning diffusion texture priors for image restoration. In *Proceedings of the IEEE/CVF conference on computer vision and pattern recognition*, pages 2524–2534, 2024. 1

[108] Conghan Yue, Zhengwei Peng, Junlong Ma, Shiyan Du, Pengxu Wei, and Dongyu Zhang. Image restoration through generalized ornstein-uhlenbeck bridge. *arXiv preprint arXiv:2312.10299*, 2023. 7

[109] Huanjing Yue, Yijia Cheng, Yan Mao, Cong Cao, and Jingyu Yang. Recaptured screen image demoiréing in raw domain. *IEEE Transactions on Multimedia*, 25:5589–5600, 2022. 6, 7, 16

[110] Syed Waqas Zamir, Aditya Arora, Salman Khan, Munawar Hayat, Fahad Shahbaz Khan, Ming-Hsuan Yang, and Ling Shao. Multi-stage progressive image restoration. In *Proceedings of the IEEE/CVF conference on computer vision and pattern recognition*, pages 14821–14831, 2021. 18

[111] Syed Waqas Zamir, Aditya Arora, Salman Khan, Munawar Hayat, Fahad Shahbaz Khan, and Ming-Hsuan Yang. Restormer: Efficient transformer for high-resolution image restoration. In *Proceedings of the IEEE/CVF conference on computer vision and pattern recognition*, pages 5728–5739, 2022. 7, 18

[112] Syed Waqas Zamir, Aditya Arora, Salman Khan, Munawar Hayat, Fahad Shahbaz Khan, Ming-Hsuan Yang, and Ling Shao. Learning enriched features for fast image restoration and enhancement. *IEEE transactions on pattern analysis and machine intelligence*, 45(2):1934–1948, 2022. 18

[113] Haijin Zeng, Xiangming Wang, Yongyong Chen, Jingyong Su, and Jie Liu. Vision-language gradient descent-driven all-in-one deep unfolding networks. In *Proceedings of the Computer Vision and Pattern Recognition Conference*, pages 7524–7533, 2025. 7

[114] Jinghao Zhang, Jie Huang, Mingde Yao, Zizheng Yang, Hu Yu, Man Zhou, and Feng Zhao. Ingredient-oriented multi-degradation learning for image restoration. In *Proceedings of the IEEE/CVF conference on computer vision and pattern recognition*, pages 5825–5835, 2023. 1

[115] Kai Zhang, Wangmeng Zuo, and Lei Zhang. Ffdnet: Toward a fast and flexible solution for cnn-based image denoising. *IEEE Transactions on Image Processing*, 27(9):4608–4622, 2018. 1

[116] Kai Zhang, Yawei Li, Jingyun Liang, Jie Zhang, Cao, Yulun Zhang, Hao Tang, Deng-Ping Fan, Radu Timofte, and Luc Van Gool. Practical blind image denoising via swin-conv-unet and data synthesis. *Machine Intelligence Research*, 20(6):822–836, 2023. 1

[117] Lvmin Zhang, Anyi Rao, and Maneesh Agrawala. Adding conditional control to text-to-image diffusion models. In *Proceedings of the IEEE/CVF international conference on computer vision*, pages 3836–3847, 2023. 2

[118] Richard Zhang, Phillip Isola, Alexei A Efros, Eli Shechtman, and Oliver Wang. The unreasonable effectiveness of deep features as a perceptual metric. In *Proceedings of the IEEE conference on computer vision and pattern recognition*, pages 586–595, 2018. 6

[119] Xu Zhang, Jiaqi Ma, Guoli Wang, Qian Zhang, Huan Zhang, and Lefei Zhang. Perceive-ir: Learning to perceive degradation better for all-in-one image restoration. *IEEE Transactions on Image Processing*, 2025. 1, 2, 7

[120] Xu Zhang, Huan Zhang, Guoli Wang, Qian Zhang, and Lefei Zhang. Clearair: A human-visual-perception-inspired all-in-one image restoration. *arXiv preprint arXiv:2601.02763*, 2026. 1, 2

[121] Yuhong Zhang, Hengsheng Zhang, Xinning Chai, Zhengxue Cheng, Rong Xie, Li Song, and Wenjun Zhang. Diff-restorer: Unleashing visual prompts for diffusion-based universal image restoration. *arXiv preprint arXiv:2407.03636*, 2024. 2, 4

[122] Dian Zheng, Xiao-Ming Wu, Shuzhou Yang, Jian Zhang, Jian-Fang Hu, and Wei-Shi Zheng. Selective hourglass mapping for universal image restoration based on diffusion model. In *Proceedings of the IEEE/CVF conference on computer vision and pattern recognition*, pages 25445–25455, 2024. 7, 18

[123] Naishan Zheng, Man Zhou, Yanmeng Dong, Xiangyu Rui, Jie Huang, Chongyi Li, and Feng Zhao. Empowering low-light image enhancer through customized learnable priors. In *Proceedings of the IEEE/CVF International Conference on Computer Vision*, pages 12559–12569, 2023. 1

[124] Yuqian Zhou, David Ren, Neil Emerton, Sehoon Lim, and Timothy Large. Image restoration for under-display camera. In *Proceedings of the ieee/cvf conference on computer vision and pattern recognition*, pages 9179–9188, 2021. 17

[125] Kaiwen Zhu, Jinjin Gu, Zhiyuan You, Yu Qiao, and Chao Dong. An intelligent agentic system for complex image restoration problems. *arXiv preprint arXiv:2410.17809*, 2024. [7](#)

# TPGDiff: Hierarchical Triple-Prior Guided Diffusion for Image Restoration

## Supplementary Material

### A. Diffusion-based Image Restoration.

We adopt IR-SDE [55] as the base diffusion framework to model the continuous stochastic evolution from high-quality images to degraded low-quality images. IR-SDE formulates image degradation via stochastic differential equations (SDEs), which naturally casts image restoration as a reverse diffusion process. The forward diffusion process is defined as:

$$dx = \theta_t(\mu - x) dt + \sigma_t dw, \quad (1)$$

where  $\mu$  denotes the state mean;  $\theta_t$  and  $\sigma_t$  are time-dependent positive functions that control the mean-reversion rate and noise intensity, respectively; and  $w$  denotes a standard Wiener process.

When the SDE coefficients satisfy  $\sigma_t^2/\theta_t = 2\lambda^2$ , the marginal distribution  $p_t(x)$  of the forward process admits an analytical form at any time  $t$  [55]:

$$p_t(x) = \mathcal{N}(x(t) | m_t, v_t), \quad (2)$$

where the mean and variance are given by:

$$m_t := \mu + (x(0) - \mu) \exp(-\bar{\theta}_t), \quad (3)$$

$$v_t := \lambda^2(1 - \exp(-2\bar{\theta}_t)), \quad (4)$$

with  $\bar{\theta}_t := \int_0^t \theta_z dz$ . As time  $t$  increases,  $m_t$  and  $v_t$  converge to  $\mu$  and  $\lambda^2$ , respectively. Therefore, the forward process can be interpreted as the initial state  $x(0)$  gradually evolving toward  $\mu$  under a mean-reverting force, while being perturbed by Gaussian noise with strength  $\lambda$ .

The forward process in Eq. (1) is an Itô SDE defined in forward time. Its corresponding reverse-time form can be derived following [79] as:

$$dx = [\theta_t(\mu - x) - \sigma_t^2 \nabla_x \log p_t(x)] dt + \sigma_t dw, \quad (5)$$

where  $\hat{w}$  denotes a Wiener process in reverse time.

During training, since the high-quality image  $x(0)$  is directly accessible, the true score function  $\nabla_x \log p_t(x)$  can be computed analytically from the marginal distribution in Eq. (2):

$$\nabla_x \log p_t(x) = -\frac{x(t) - m_t}{v_t}. \quad (6)$$

By reparameterization,  $x(t)$  can be expressed as:

$$x(t) = m_t(x) + \sqrt{v_t} \epsilon_t, \quad (7)$$

where  $\epsilon_t \sim \mathcal{N}(0, \mathbf{I})$  is standard Gaussian noise. Accordingly, the score function can be equivalently written as:

$$\nabla_x \log p_t(x) = -\frac{\epsilon_t}{v_t}. \quad (8)$$

In practice, a neural network is employed to predict this noise term. At inference time, by numerically solving the reverse SDE, the low-quality image is progressively mapped back to the high-quality image. This procedure is consistent with existing diffusion-based image restoration methods.

### B. More Details About Datasets.

In this section, We provide a detailed description of the degradation datasets used in this paper. Both our approach and the selected comparative methods were uniformly trained and tested on these datasets. Specific dataset details are as follows:

## B.1. Single-task image restoration datasets

- **Low-Light Enhancement:** Images are collected from the LOL-V2 [105] dataset, which contains 689 paired training images and 100 paired testing images.
- **Non-Homogeneous Dehazing:** Images are collected from the NH-HAZE [3] dataset, and we adopt a customized split with 49 images for training and 6 images for testing.
- **Demoire:** Images are collected from the RAW image demoireing dataset used for RDNet [109], which contains 2,979 randomly selected paired training images and 408 paired testing images.
- **Deraining:** Images are collected from the Rain100L [103] dataset, which contains 2103 paired training images and 1111 paired testing images.
- **Desnowing:** Images are collected from the desnowing task subset of the WeatherBench [24] dataset, which contains 13,059 paired training images and 200 paired testing images.
- **Dehazing:** Images are collected from the RESIDE6K [68] dataset, which contains 6,000 paired training images and 1,000 paired testing images.
- **Raindrop Removal:** Images are collected from the RainDrop [67] dataset, which contains 861 paired training images and 58 paired testing images.
- **Defocus Deblurring:** Images are collected from the DPDD [1] dataset, which contains 350 paired training images and 76 paired testing images.
- **Declouding:** Images are collected from the RS-Cloud [63] dataset, which contains 485 paired training images and 15 paired testing images.

## B.2. Multi-task All-in-one Image Restoration Datasets

- **5D All-in-one Image Restoration Datasets:** For the unified 5D image restoration setting, multiple public benchmarks are adopted to cover diverse degradation types. Specifically, the LOL-v1 [93] dataset is used for low-light image enhancement, which contains 485 paired training images and 15 paired testing images. The GoPro [62] dataset is employed for single-image motion deblurring, consisting of 2,103 training images and 1,111 testing images. For rain streak removal, the Rain100L [103] dataset provides 200 paired training images. The RESIDE [37] dataset is used for image dehazing, where 72,135 training images are utilized and 500 testing images are selected from the SOTS subset. For Gaussian denoising, a total of 5,144 training images are collected from BSD400 [58] and WED [57], while BSD68 [58], containing 68 images, is used for evaluation.

## C. More Experimental Details

### C.1. Network Depth Partition: Shallow vs. Deep Layers

To explicitly address the hierarchical differences within the U-Net architecture, we partition the network into *shallow* and *deep* layers based on spatial resolution and semantic abstraction levels. The partition is defined by the downsampling factor relative to the input resolution. Let  $i \in \{0, 1, \dots, D-1\}$  denote the stage index of the encoder, where stage  $i$  has a spatial resolution of  $H/2^i \times W/2^i$ .

**Shallow Layers.** Shallow layers correspond to the early stages of the encoder and the late stages of the decoder. These layers operate at high spatial resolutions and are responsible for processing local geometric structures and fine-grained details.

$$\mathcal{S} = \{\text{Stage } k \mid \text{Resolution}(k) \geq \frac{H}{4} \times \frac{W}{4}\} \quad (9)$$

Given the discrete resolution hierarchy of the U-Net, this definition corresponds to encoder stages  $i \in \{0, 1, 2\}$  in our implementation ( $D = 4$ ).

**Deep Layers.** Deep layers include encoder stages with  $i \geq 3$ , the bottleneck, and their symmetric decoder counterparts. These layers operate at low spatial resolutions, where the receptive field is sufficiently large to capture global context and high-level semantic information.

$$\mathcal{D} = \{\text{Stage } k \mid \text{Resolution}(k) \leq \frac{H}{8} \times \frac{W}{8}\} \quad (10)$$

This corresponds to encoder stages  $i \geq 3$  and the bottleneck under the same configuration. The decoder follows a symmetric partition strategy. Table 5 summarizes the classification of all network stages.

Table 5. Definition of Shallow and Deep Layers Based on Spatial Hierarchy in the U-Net Backbone.

Component	Spatial Size	Category	Dominant Feature Type
Encoder ( $i = 0, 1, 2$ )	High	Shallow	Local Texture
Encoder ( $i \geq 3$ )	Low	Deep	High-level Semantics
Bottleneck	Lowest	Deep	Global Context
Decoder ( $j \leq D - 4$ )	Low	Deep	Semantic Reconstruction
Decoder ( $j \geq D - 3$ )	High	Shallow	Detail Refinement

## D. Additional Experimental Results.

### D.1. Unknown Task Generalization

To evaluate the generalization robustness of TPGDiff under unseen and complex degradation conditions, we conduct quantitative experiments on the POLED and TOLED datasets [124]. These datasets, captured by under-display cameras, present significant challenges due to their high-resolution nature and intertwined real-world artifacts that differ from synthetic training distributions. As summarized in Table 6, our method consistently surpasses existing benchmarks across multiple evaluation metrics. This superior performance in cross-domain scenarios underscores the efficacy of our triple-prior guidance, which provides a generalized structural and semantic framework that remains effective even when encountering novel degradation characteristics.

### D.2. Error Analysis of Prior Injection Positions

In this part, we further analyze the error distribution characteristics of semantic and structural priors when injected at different network hierarchies. Figure 6 visualizes the per-pixel error maps under different prior injection strategies. It can be observed that when semantic priors are injected into shallow layers or structural priors are injected into deep layers, pronounced high-error responses emerge in regions with dense rain/snow streaks as well as around structural edges (highlighted by red boxes). This phenomenon indicates a mismatch between the injected priors and the representational capacity of different network layers. In contrast, injecting semantic priors into deep layers while applying structural priors to shallow layers effectively suppresses the spatial concentration of errors and leads to a lower overall error magnitude.

## E. Additional Visual Results.

### E.1. Visualization Results for Single-Task Learning

In this subsection, we present additional qualitative restoration results of our model under the single-task setting. As shown in Figure 7, we provide direct comparisons among the low-quality input images (LQ), the restored results produced by our method (Ours), and the corresponding ground-truth images (GT) across nine tasks, including deraining, declouding, raindrop removal, low-light enhancement, desnowing, defocus deblurring, motion deblurring, water ripple removal, and dehazing. The results demonstrate that, despite severe quality degradation in the input images, our model is able to accurately reconstruct sharp edge structures and faithfully recover realistic texture details.

### E.2. Visualization Results for Multi-Task Learning

To further validate the generality and robustness of the proposed model, this subsection presents qualitative comparisons under the multi-task joint training setting. As shown in Figs. 8 to 12, we compare our method with existing approaches on representative tasks including deraining, denoising, low-light enhancement, and deblurring. The results indicate that existing methods tend to suffer from over-smoothing or residual artifacts when confronted with complex and diverse degradation scenarios, making it difficult to balance noise removal and detail preservation. In contrast, our approach, benefiting from a unified multi-task learning framework, demonstrates robust restoration performance across various degradation types.

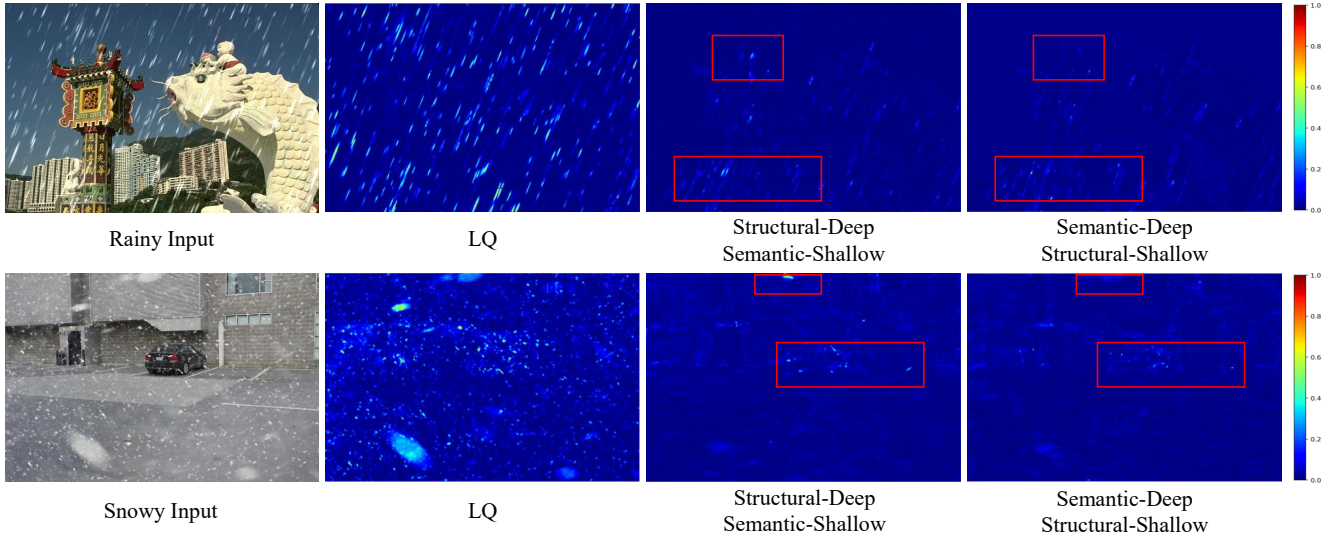


Figure 6. Per-pixel error distribution maps under different prior injection hierarchies. The injection of semantic and structural priors at different network layers has a significant impact on the error distributions in rain/snow regions and along structural edges.

Table 6. Comparison under unknown tasks setting (under-display camera image restoration) on TOLED and POLED datasets.  $\uparrow$  represents the bigger the better, and  $\downarrow$  represents the smaller the better. Best and second-best results are highlighted in red and blue, respectively.

Method	POLED			TOLED		
	PSNR $\uparrow$	SSIM $\uparrow$	LPIPS $\downarrow$	PSNR $\uparrow$	SSIM $\uparrow$	LPIPS $\downarrow$
HINet [9]	11.52	0.436	0.831	13.84	0.559	0.448
MPRNet [110]	8.34	0.365	0.798	24.69	0.707	0.347
SwinIR [45]	6.89	0.301	0.852	17.72	0.661	0.419
DGUNet [60]	8.88	0.391	0.810	19.67	0.627	0.384
NAFNet [10]	10.83	0.416	0.794	26.89	0.774	0.346
MIRV2 [112]	10.27	0.425	0.722	21.86	0.620	0.408
Restormer [111]	9.04	0.399	0.742	20.98	0.632	0.360
RDDM [47]	15.58	0.398	0.544	23.48	0.639	0.383
DL [22]	13.92	0.449	0.756	21.23	0.656	0.434
TAPE [48]	7.90	0.219	0.799	17.61	0.583	0.520
AirNet [38]	7.53	0.350	0.820	14.58	0.609	0.445
DA-CLIP [54]	14.91	0.475	0.739	15.74	0.606	0.472
DiffUIR [122]	15.62	0.424	0.505	29.55	0.887	0.281
DeepSN-Net [20]	10.20	0.411	0.534	17.39	0.576	0.303
MaIR [40]	11.07	0.423	0.529	23.64	0.770	0.271
AWRaCLE [73]	11.21	0.431	0.513	10.54	0.495	0.331
Ours	15.64	0.511	0.644	32.70	0.899	0.145

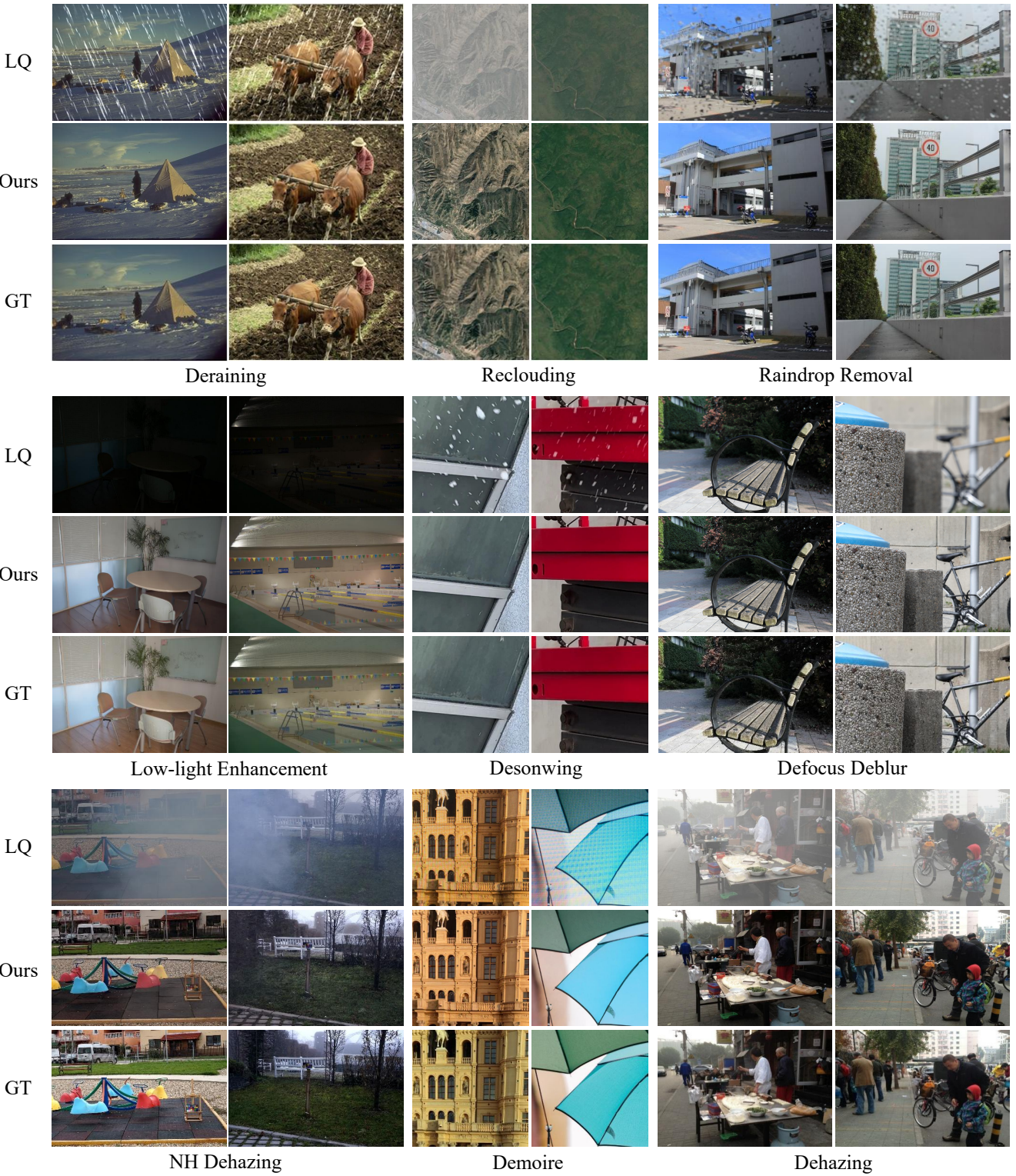


Figure 7. Visual results of applying our TPGDiff to various degradation recovery tasks, demonstrating a unified model capable of addressing multiple degradation types. Zoom in for best view.

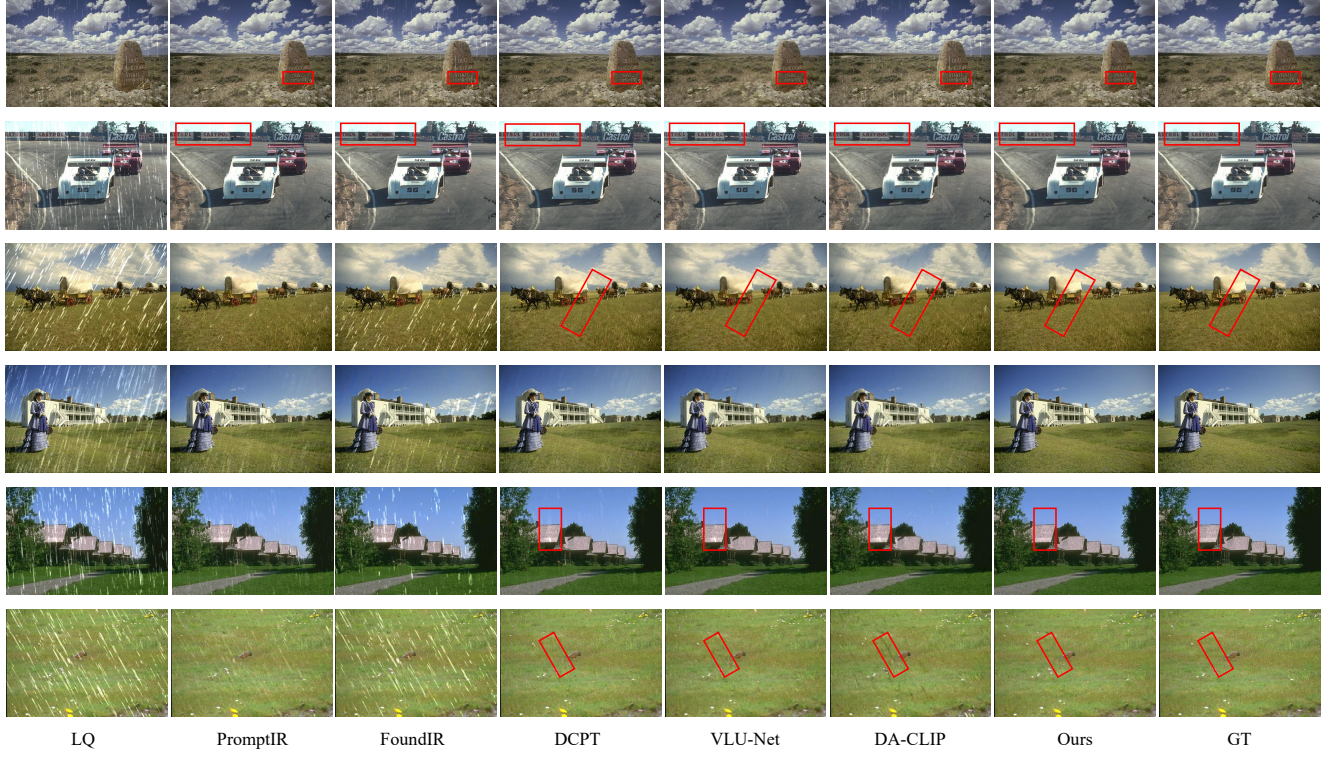


Figure 8. Visualization results for the image deraining task under different methods on the Rain100L dataset. Zoom in for best view.

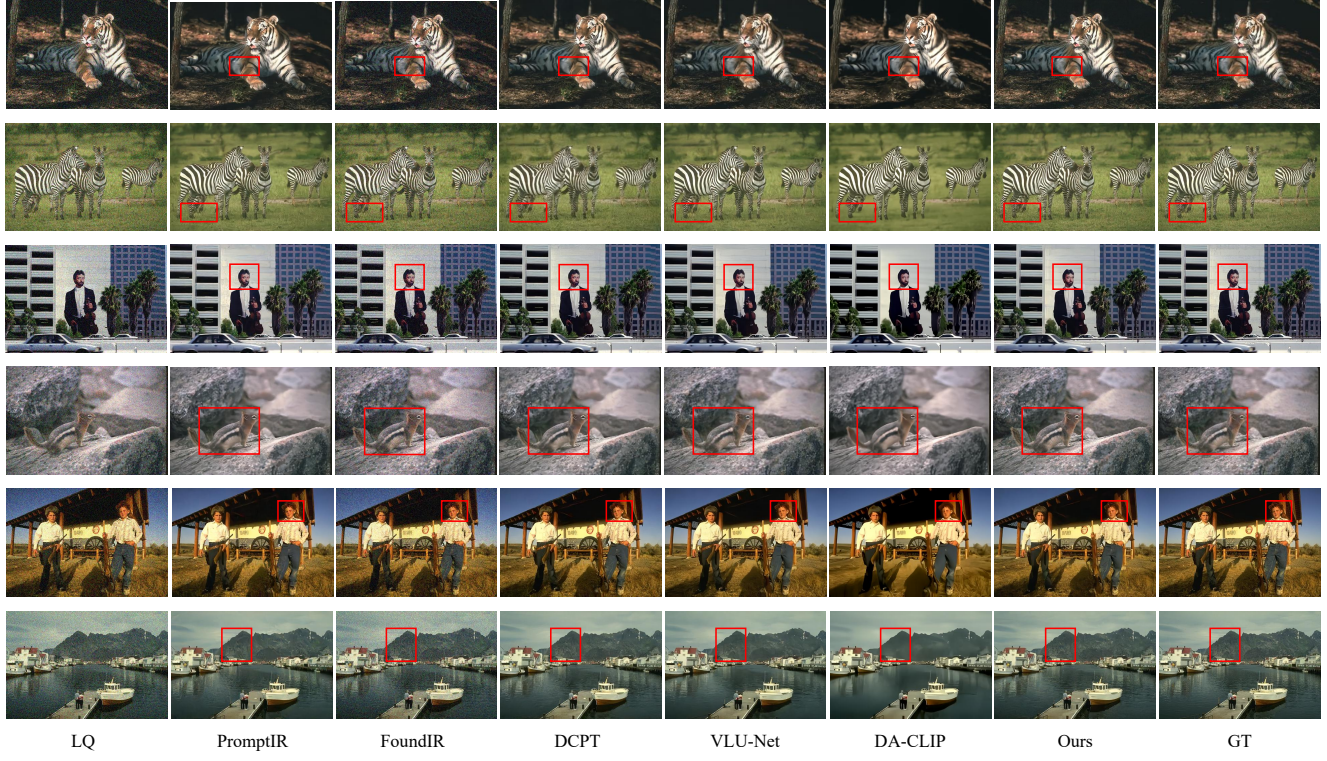


Figure 9. Visualization results for the image denoising task under different methods on the CBSD68 dataset. Zoom in for best view.

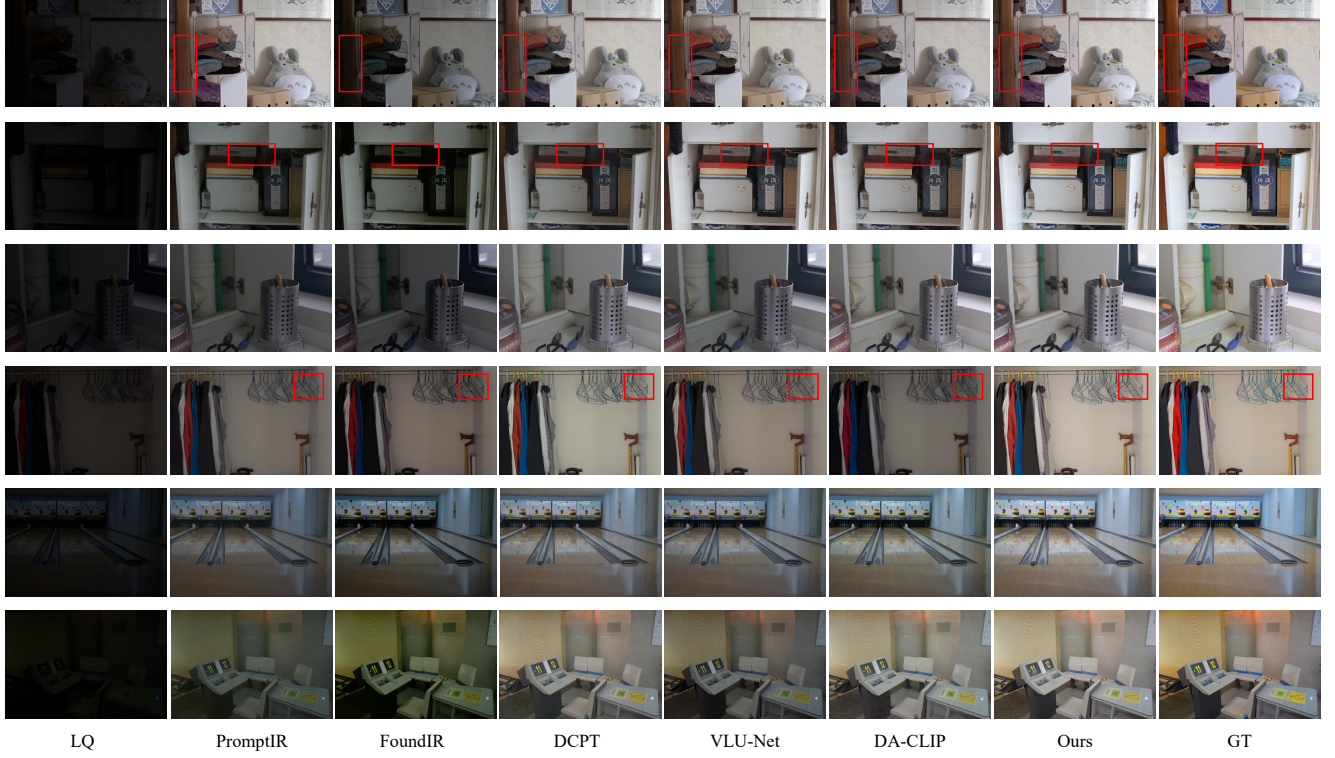


Figure 10. Visualization results for the low-light image enhancement task under different methods on the LOL-v1 dataset. Zoom in for best view.

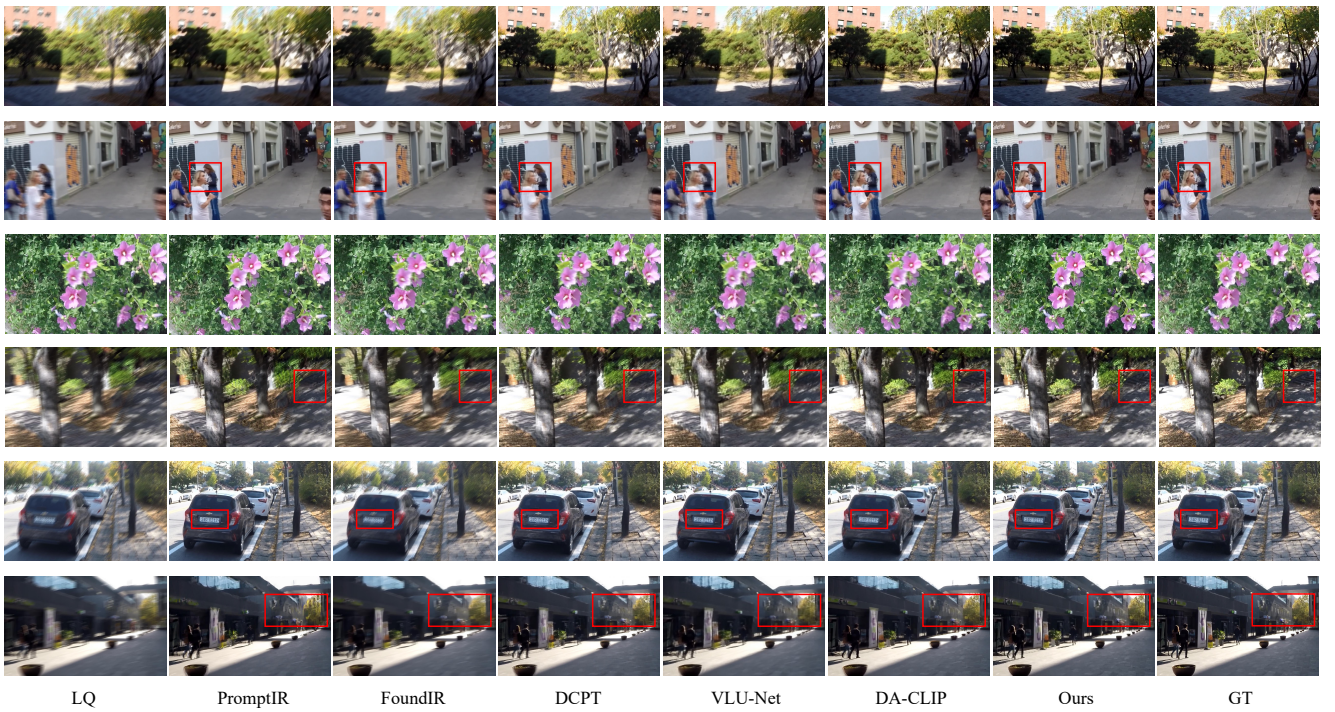


Figure 11. Visualization results for the image deblurring task under different methods on the GoPro dataset. Zoom in for best view.



Figure 12. Visualization results for the image dehazing task under different methods on the SOTS dataset. Zoom in for best view.